Cement and Concrete Research 199 (2026) 108036

Contents lists available at ScienceDirect

Cement and Concrete Research

journal homepage: www.elsevier.com/locate/cemconres

Low-grade kaolinitic clays as SCMs for low-carbon cements and strength improvement by C-S-H gel nucleation seeding

Diego Vallina [a,b], Isabel Santacruz [a,b,*], Alejandro Morales-Cantero [a,b], María Dolores Rodríguez-Ruiz [a], Ana Cuesta [a,b], Angeles G. De la Torre [a,b], Alessandro Dalla-Libera [c], Pere Borralleras [d], Sébastien Dhers [e], Peter Schwesig [e], Oliver Mazanec [e], Miguel A.G. Aranda [a,b,*]

[a] Departamento de Química Inorgánica, Cristalografía y Mineralogía, Universidad de Málaga, Málaga, 29071, Spain
[b] Instituto Universitario de Materiales y Nanotecnología, IMANA, Universidad de Málaga, Málaga, 29071, Spain
[c] Master Builders Solutions Italia Spa, Via Vicinale delle Corti, 21, 31100 Treviso, Italy
[d] Master Builders Solutions España S.L.U., Carretera de l'Hospitalet, 147-149, Edificio Viena, 1ª planta, 08940 Cornellà de Llobregat, Spain
[e] Master Builders Solutions Deutschland GmbH, Albert-Frank Str. 32, 83308 Trostberg, Germany

ARTICLE INFO

Keywords:
LC^3-50
Low-grade kaolinite clays
Thermal activation
C-S-H gel nucleation seeding
Performances

ABSTRACT

This study seeks to push the limits of LC^3-50 binders by utilising low-grade kaolinite clays and C-S-H gel nucleation seeding. Four commercially-available kaolinite clays (i.e. kaolinite contents ~20 wt%) have been studied by X-ray fluorescence, X-ray powder diffraction and thermal analysis. The clays were thermally activated and milled to $D_{v,50} = 11 \pm 2$ μm. The activated clays showed low pozzolanic performances, as determined by ASTM C1897-20 standard. The heat flows ranged 200–230 J/g calcined clay and the bound waters 4.3–5.7 %. The LC^3-50 pastes were characterised by calorimetry, X-ray powder diffraction and the Rietveld method, thermal analysis, and porosimetry to evaluate pozzolanic reactivity and the seeding effect.

LC^3 mortars, w/b = 0.40, have relatively low compressive strengths, especially at one day, but these values were increased by 64 % on average at one day by seeding. At 1 day, three LC^3 mortars showed 11 MPa which increased to 18–20 MPa by seeding. A fourth mortar showed a much higher compressive strength, 16 MPa, that increased to 23 MPa, by seeding. A tested concrete, w/b = 0.50, also showed a high increase of 37 % at 1 day. The improvements at 28 days were maintained but quantitatively lower, 12 and 14 % for the mortars and the concrete, respectively. Insights into the pozzolanic reactions and C-S-H seeding are obtained from the quantitative study of the pastes. For instance, it is proven the pozzolanic reaction at 1 day from the portlandite consumption. Also shown is the enhanced formation of carboaluminates when the strength enhancing admixture is added.

1. Introduction

Partial replacement of clinker with supplementary cementitious materials (SCMs) is a well-established strategy to reduce the environmental footprint of cement production. Currently, most cements are blended with SCMs such as fly ash (FA), blast furnace slag (BFS), and limestone (LS). While these SCMs can produce high-quality low-carbon cements, the long term availability of FA and BFS is dubious due to the decarbonisation initiatives of the corresponding industries [1]. Limestone calcined clay cement (LC^3-50) is a relatively new blended cement, that typically consists of 50 wt% Portland clinker, 30 wt% calcined clay, 15 wt% LS, and ~5 wt% gypsum, enabling a reduction in CO_2 emissions of approximately 40 % compared to PC type I [2]. LC^3 complies with the new European standard for composite Portland cement (EN-UNE 197-5) classified as CEM II/C-M (Q-L(L)), enabling the reduction of clinker content to 50 wt% [3]. Although there are some studies of LC^3-binders prepared with different calcined clays [4], such as smectite [5], or muscovite/illite [6], LC^3 are usually prepared with kaolinite (kln) calcined clays, as they give the highest performances. The synergism between clinker, calcined clay, and LS makes these blends competitive from 3 to 7 days of hydration. This is chiefly possible due to: i) the fast hydration/reaction kinetics of metakaolin (MK), i.e. $Al_2Si_2O_7$, which is

* Corresponding authors at: Departamento de Química Inorgánica, Cristalografía y Mineralogía, Universidad de Málaga, Málaga, 29071, Spain.
E-mail addresses: isantacruz@uma.es (I. Santacruz), g_aranda@uma.es (M.A.G. Aranda).

https://doi.org/10.1016/j.cemconres.2025.108036
Received 9 December 2024; Received in revised form 15 May 2025; Accepted 2 September 2025
Available online 24 September 2025

the main active component after calcination of kaolinitic clays; ii) the pozzolanic reaction of MK with the portlandite produced during clinker hydration, to form C-A-S-H gel with variable stoichiometry close, to $Ca_{1.5}Al_{0.2}SiO_{3.8}(H_2O)_{4.0}$; iii) the reaction of the remaining aluminium from the MK with the carbonate anions from LS to form carboaluminate hydrates, and iv) the filler effect of the LS and the remaining phases of the calcined clay. Calcined clays promote the precipitation of AFm-type phases and C–A–S–H with longer chains, where aluminium substitutes for silicon [7]. The pozzolanic reactions that happen during the hydration of LC^3 are thoroughly discussed in other studies [8–11]. These reactions enable LC^3 to attain mechanical properties to those of type I PC after approximately 3 days of hydration, even with higher levels of clinker substitution compared to other SCMs [12].

Kaolin can be defined as a rock with kaolinite-group minerals, accompanied with other minerals, such as quartz, feldspar and mica [13]. Being a natural material, clay rocks frequently contain impurities, such as anatase, calcite, hematite, pyrite, and so on. Some impurities can negatively affect the pozzolanic activity of the clay after calcination, as happens with CaO (formed from $CaCO_3$ thermal decomposition), because it reduces the formation of MK above 800 °C [14]. Additionally, clays rich in pyrite can release SO_3 during calcination, which has detrimental effects on both the calcined clay and the environment [14]. However, the impact of other impurities depends on their concentration in the clay. For example, while 2.7 wt% Fe_2O_3 resulted in a more compact cement structure associated with an enhanced pozzolanic reaction and a higher consumption of portlandite, higher levels may have a detrimental impact [15]. Certain oxides, such as Na_2O and K_2O can also act as fluxing agents, reducing the specific surface area of the calcined clay and thereby lowering its reactivity at early ages [16]. Clays need to be activated, usually by calcination, before being used in LC^3 binders. Clay calcination is accomplished by the dehydroxylation, while preventing (re)crystallisation at higher temperatures. Thus, the ideal activation temperature range falls between these two processes, dehydroxylation and (re)crystallisation of new mineral phases, between 600 °C and 900 °C for kln [17]. The highest pozzolanic reactivity is attained when the clay is calcined at the temperature where an optimal balance between specific surface area and structural disorder is achieved [7]. The key parameters to have fast pozzolanic reactivity of the meta-clay phase, i.e. MK, at early hydration ages, are surface area, particle size, and structural disorder [18]. However, at later ages (i.e. more than 7 days), the MK content is the main parameter to justify the mechanical strengths of the resulting mortars [19]. The rheological properties, and consequently, the superplasticiser (SP) dosage, are usually correlated with the metakaolin content; however, there are other parameters, such as the specific surface area [20] and the particle shape [21] of the calcined clays that also have an effect. Other factors may also influence the SP demand, such as the iron content of the SCM, although further research is required to confirm this [20]. The MK content in the calcined clay has been shown to affect not only the rheological behaviour but also the strength development [19,22]. For the former, the amount of SP needed usually increases by increasing the metakaolin content for the same flowability [22]; and for the latter, for LC^3-50 systems, at least 40 wt% MK containing calcined clays are needed (if strength enhancing admixtures are not used) [19,22]. LC^3 mortars and concretes prepared with clays that contain 40–50 wt% kln usually present good workability, competitive mechanical strengths after three days, together with a very good chloride penetration resistance [23]. However, it is known that LC^3 systems have poorer carbonation resistance than Portland Cement (PC) [22]. Consequently, the use of medium-grade kln clays (40–60 wt% kln) represents a cost-effective alternative to high-grade clays (>60 wt% kln). A smooth, nearly linear relationship exists between the mechanical strength and the amount of MK in the calcined clay.

To ensure competitive performances, i.e. kln contents higher than 40 wt%, the LC^3 consortium recommends [14] the chemical criteria shown in Table 1. The theoretical criteria correspond to a material with a composition close to 40 wt% of kln and 60 wt% of quartz. The empirical criteria are related to the values from the chemical composition and experience of the authors. In addition, low amounts of CaO and SO_3 are recommended, as detailed above.

Table 1
Setting chemical criteria (in wt%) to select raw clays with ≥40 wt% kaolinite [14].

Theoretical criteria	Empirical criteria	Additional criteria
% Al_2O_3 = 15.8 Al_2O_3 / SiO_2 = 0.2	% Al_2O_3 ≥ 18.0 Al_2O_3 / SiO_2 ≥ 0.3 % LOI ≥ 7.0 % Na_2O_{eq} < 3.0	% CaO < 3.0 (low calcite) % SO_3 < 3.0 (low sulfate / sulfide)

However, factors like the accessibility, cost of raw materials and transportation are crucial determinants. Indeed, many cement plants do not have deposits of medium-grade kln clays nearby, therefore, based on the location of the cement plant, the use of alternative clays [4], such as smectite, illite/muscovite may be considered. Another alternative could be the use of low-grade kln clays, i.e. with kln contents lower than 30 wt %, which, although they do not fulfil the criteria shown in Table 1, are available close by. Recently, a few articles focusing on the potential utilisation of low-grade kaolinitic calcined clays as SCM have been published [24–33]. However, there are two challenges associated with this type of material that make comparisons difficult. The first challenge is the difficulty in accurately estimating the percentage of kln in the clay when it is present in low amounts. The second challenge arises from the fact that, as natural materials, these clays often contain other pozzolanic phases, such as smectite or illite, in varying percentages. A smart way to circumvent these problems is to use the ASTM C1897 pozzolanic activity [34] as reported by [35]. A high purity MK sample gave 1150 J/g of SCM of cumulative heat at seven days, and activated low-grade kaolinitic clays gave 230–330 J/g of SCMs [35]. Independent works reported 1030 and 1085 J/g of pure MK in [36] and [18], respectively. Therefore, by assuming an average heat of 1100 J/g of pure MK, the 30 % MK content would yield a threshold of 330 J/g of SCMs. Therefore, low-grade kaolinitic clays can also be classified as those yielding less than 330 J/g of SCMs.

It should be noted that in the ten scientific papers dealing with low-grade kaolinitic clays, there is no approach that uses accelerators/strength enhancing admixtures. In fact, just two report the pozzolanic activities according to ASTM C1897 standard [31,33]. In [31], the reported heat released at 7 days was 180 J/g SCM and the resulting LC^3-50 mortars (w/b = 0.40 with a PC-52.5R) showed 30 and 46 MPa (compressive strength values) at 7 and 28 days, respectively. In [33], the heat released was 329 J/g and the resulting LC3-50 mortars (w/b = 0.40 with a PC-42.5R) had 40 and 46 MPa at 7 and 28 days, respectively. The mechanical strengths at one day were not reported.

C-S-H nanoparticle nucleation seeding has two main effects on cement hydration [37–39], chemistry-related and physics-related. From the chemistry viewpoint, these nanoparticles modify the pore solution concentrations (e.g. SO_4^{2-}, Ca^{2+}, Al^{3+}, etc.), as these ions are adsorbed because the very large surfaces of the nanoparticles. In turn, the adsorption of ions has three main effects: i) it creates local concentration gradients that alters the dissolution pathways, ii) the C-S-H growth mechanism, from alite hydration and from the pozzolanic reaction, could be changed due to the adsorbed species, and iii) the changes in SO_4^{2-} and Al^{3+} concentrations indirectly modify, it could even delay, alite dissolution. The roles of aluminate [40–44] and sulfate [45,46] species in alite hydration rate are being very actively researched. If alkanolamines are included within the admixtures, the ferrite phase hydration is accelerated [8,47–49]. This contributes to expose additional alite surfaces to hydration during early ages [50], when there is plenty of water for hydration. This enhances cement hydration at the key early age because of the intergrown nature of the alite/ferrite components. All these effects are not directly related to the nucleation process.

From the physics viewpoint, C-S-H nanoparticle seeding provides

very effective additional nucleation sites. There are two different consequences from this effect. On the one hand, it initially accelerates calcium silicate hydration, also known as the filler effect [51–53]. This is because of the connection between alite dissolution and C-S-H gel precipitation. On the other hand, synchrotron imaging techniques have shown that C-S-H seeding partly moves the C-S-H precipitation and growth away from the dissolving alite particles, enhancing secondary nucleation in the capillary porosity [54,55]. The rearrangement of the C-S-H gel from the surfaces of alite particles (inner C-S-H gel with higher mass density) to the pore space (outer C-S-H gel with lower mass density) leads to a more homogeneous C-S-H distribution in the bulk of the paste [56], which in turn decreases the porosity, improving the mechanical strengths, and reducing the permeability of the final binder [57]. This has also been indirectly evidenced by lower porosities and smaller threshold pore entry sizes, as measured by MIP. It should be noted that C-S-H densities at the microscale can span from lower than 1.80 gcm^{-3} (outer C-S-H with larger content of gel pore water) to higher than 2.10 gcm^{-3} (inner C-S-H with smaller amount of gel pore water), i.e. up to a 15 % difference. Therefore, even with the same degree of hydration, a larger fraction of outer C-S-H gel leads to lower porosities and, chiefly, higher connectivities [55].

In this study, we address the knowledge gap for LC^3 binders based on low-grade kaolinitic clays. We push the limits of LC^3-50 binders by utilising four commercially available low-grade kaolinitic clays without measurable amounts of smectite. These low carbon cements are economically quite competitive but their hydration kinetics are slow because the MK contents. LC^3 mortars, w/b = 0.40, containing C-S-H gel nucleation seeding gave competitive compressive strengths, as they increased by ~60 % at one day of hydration when compared to the unseeded mortars. The compressive strength of one concrete, w/b = 0.50, has also been studied and C-S-H gel nucleation seeding boosted its one-day compressive strength by 37 %. The mechanisms underlying the pozzolanic reaction and the seeding are studied for the corresponding LC^3 pastes.

2. Materials and methods

2.1. Starting material

In this work, four commercial low-grade Spanish kaolinite clays (designated as **RCx**) have been studied: **RC1** from Badajoz was provided by Arcillas La Serena S.L.; **RC2** from Seville was supplied by Refractarios Andalucía S.L.; and **RC3** and **RC4** were supplied by Arcillas Moreno S.L., and they are from Albacete and Valencia, respectively.

Additionally, two reference Spanish clays from Guadalajara, supplied by Caobar S.A., were used as medium-grade kaolinite clays (Caolin C/N-2021 and Caolin C-2021), hereinafter referred to as RC_{ref1} and RC_{ref2}, respectively.

Portland cement (PC), classified as CEM I 52.5 R in accordance with the EN 197-1 standard, with a particle size ($D_{v,50}$) of ~12 μm, was employed (PC-525). This cement was supplied by Cementos Cosmos, Votorantim Cimentos Group (Malaga, Spain). A commercial limestone (LS), Omyacarb®5F, was supplied by Omya Clariana S.L.U. (Granada, Spain), and commercial gypsum (Gy) was provided by Fábrica de Yesos y Escayolas La Maruxiña S.A. (Toledo, Spain). The gypsum was ground in the laboratory to a particle size ($D_{v,50}$) of ~13 μm, as detailed in [8]. The elemental compositions and textural properties of PC, LS, and Gy have been previously reported [8].

As superplasticiser (**SP**), a commercial polycarboxylate-based SP was used, MasterCO_2re 3240, supplied by Master Builders Solutions, with a solids content of 35 wt%. It was specifically designed to avoid fluidity loss during the early stages of low-carbon cement hydration. Furthermore, a strength-enhancing admixture, Master X-Seed STE 53, named hereafter as **STE53**, provided by Master Builders Solutions España S.L.U., was employed. This admixture contains C-S-H gel-based seeds with alkanolamines [58] and has a solids content of 28 wt%. An optimised amount of SP was used to prepare all LC^3 pastes and mortars as detailed below.

2.2. Clays calcination and milling

Both raw and calcined clays were dried at 105 °C prior to further processing/characterisation. All clays were subjected to calcination at 860 °C for 4 h in an industrial facility at a brick factory (Inducerama S.L., Spain) hereinafter referred to as **CCx**. A total of 10 kg of each clay was calcined, except for RC4, for which 100 kg were calcined. The calcined clays (CC1, CC2, and CC3) were ground using a ball mill (Proeti) with stainless steel balls, processed in 1 kg batches. In contrast, CC4 was milled using a heat able laboratory ball mill LM0504-S7 from CEMTEC, with material load ca. 12 kg. In all cases, the target average particle size was set to $D_{v,50} = 11 \pm 2$ μm.

2.3. Pastes, mortars and concrete preparation

LC^3-50 binders (hereafter named **CCx-LC^3**) consisted of 52 wt% of Portland cement (PC), 30 wt% of calcined clay (CCx), 15 wt% of limestone (LS) and 3 wt% of gypsum (Gy). Both standard and seeded pastes were prepared at 20 ± 2 °C with a water-to-binder ratio (w/b) of 0.40, using an optimised dosage of SP. Unseeded and seeded pastes were mechanically prepared (IKA, mod. RW20-D). Table S1 details the protocol followed. Seeded pastes contain 2.00 wt% (by weight of binder, bwb) of STE53. The pastes were poured into sealed Teflon cylinders (10 mm diameter × 40 mm length) and rotated for 24 h at 20 ± 2 °C. Subsequently, they were left in a saturated $Ca(OH)_2$ solution until testing at 7 and 28 days.

Mortars were prepared under the same conditions (20 ± 2 °C), following a modified EN196–1 standard. The parameters not followed have been the application of 60 knocks and the standard sand/binder ratio of 3.0. The approach used here (a self-flow of 200 mm by adding SP, and a s/b = 1.78) is related to concrete field applications and it was employed by us in several investigations [47,49,59,60]. The superplasticiser was optimised to achieve an initial self-flow of 200 ± 20 mm. The procedure for the preparation of unseeded and seeded mortars is described in Table S1. Moulds (4 × 4 × 16 cm^3) were half-filled with mortar, and 60 vertical punctures were applied using a glass rod to remove air bubbles. The moulds were then completely filled, and other 60 punctures were applied. The filled moulds were kept in a humidity chamber (20 °C, 99 % relative humidity) for 1 day, after which they were demoulded and left in tap water at 20 ± 2 °C until testing at 7 and 28 days. The water contents in the SP and STE53 admixtures were accounted for in the w/b calculations.

Concretes (C30/37, S4–5 class) were prepared using neat PC and the CC4-LC^3 binder. The dosage was 330 kg/m^3 of cement/binder, 923 kg/m^3 of silica sand (0–4 mm), 395 kg of crushed gravel (12–19 mm), 648 kg/m^3 of river gravel (25 mm) and 165 kg/m^3 of effective water, w/b = 0.50. CC4-LC^3-SP-STE53 concrete, containing the strength enhancing admixture, STE53, was fabricated by adding 2.00 wt% (bwb) of the admixture, i.e. 6.6 kg/m^3. The addition order of materials and admixtures for the unseeded and seeded concrete is described in Table S1. For this, a vertical-shaft planetary mixer, P50 by OMG SICOMA, was used (65 Hz, 1950 rpm). Concrete specimens were cast in cubic moulds (150 × 150 × 150 mm^3) and, after demoulding at one day, they were placed inside the curing room (20 ± 2 °C and > 95 % relative humidity) until further testing (i.e. 7 and 28 days).

2.4. Characterisation techniques

Prior to any characterisation, the clays were crushed, dried at 105 °C for 2 h and milled to a particle size of $D_{v,50} \sim 11 \pm 2$ μm.

2.4.1. X-ray fluorescence (XRF)

The powder samples were analysed using an ARL ADVANT'XP+

instrument from Thermo Fisher, located at the Central Research Support Service (SCAI) at the University of Malaga, with the fused bead approach. Loss on ignition (LOI) was measured by subjecting the samples to a temperature of 950 °C for 2 h.

2.4.2. Textural characterisation

Particle size distributions (PSD) were analysed by laser diffraction using a Malvern Panalytical Mastersizer 3000 instrument with a dry chamber (Aero S). The MIE non-spherical approach was utilised for data processing, and a refractive index (RI) of 1.55 was used for all the studied clays. The employed absorption indices (AI) were 0.1 and 0.01 for the four studied calcined clays and the calcined reference clays, respectively. Specific surface area (SSA) values were obtained through BET analysis of N_2 adsorption isotherms, using an ASAP 2420 instrument (Micromeritics, USA).

2.4.3. Laboratory X-ray powder diffraction (LXRPD) of clays and cement pastes

Mineralogical phase analyses were conducted using the Rietveld method with two diffractometers, both housed at the Central Research Support Service (SCAI) at the University of Málaga: (i) an X'Pert PRO MPD (PANalytical) diffractometer, configured in a Bragg-Brentano geometry and employing monochromatic CuKα_1 radiation (1.5406 Å), and (ii) a D8 ADVANCE (Bruker AXS) diffractometer, utilising monochromatic MoKα_1 radiation (0.7093 Å). To quantify the amount of amorphous and non-quantified crystalline phases (ACn), the samples were blended with 20 wt% α-Al_2O_3 as the internal standard [61]. The hydration of the pastes was not arrested using solvent exchange with the objective of minimising the decomposition of phases such as ettringite [62]. As a result, the ACn values obtained from gentle grinding with the standard include the free water. Rietveld quantitative phase analysis (RQPA) was conducted on all samples using GSAS software [63,64].

2.4.4. Pozzolanic activity ASTM C1897-20 of calcined clays (R^3 test)

The pozzolanic activity of all calcined clays was measured following the ASTM C1897-20 standard [34]. Two parameters are obtained, i.e. cumulative heat released and chemically bound water (BW). The heat released at 40 °C by a R^3-paste was measured using a calorimeter (eight-channel Thermal Activity Monitor, TAM) over a 7-day period, employing glass ampoules and water as the reference, in accordance with [65].

2.4.5. Flowability tests of mortars and concrete

The SP content was optimised through slump tests of mortars. LC^3-mortars were cast in a truncated cone mould (base and top diameters of 100 mm and 70 mm, respectively, and height of 60 mm). It was initially filled halfway, and air entrainment was minimised by performing 60 vertical punctures with a glass rod. Following this, the mould was completely filled, and another set of 60 punctures were applied. The SP dosage was optimised to achieve an initial self-flow of every mortar within 200 ± 20 mm, i.e. without any external knock. Slump flow measurements were taken immediately after preparation (t_0), and after 30 (t_{30}) and 60 min (t_{60}). Prior to the measurements at t_{30} and t_{60}, the mortars were remixed by stirring at 285 rpm for 60 s.

LC^3-concrete and the reference PC-concrete, both with SP, were poured in Abrams cone. The amount of SP was determined to keep the initial slump in the range of 210 ± 10 mm (Abrams cone slump). Initial slump and workability retention were measured following the EN 12350-2:2019 procedure.

2.4.6. Compressive strengths

An Autotest 300/20C MD2-ECO press, located at the University of Málaga, was used to measure the compressive strength of the mortars at 1, 7, and 28 days, where six half-prisms were tested for each age. Consequently, the compressive strengths given in this work are the mean of six individual measurements. For concrete characterisation, 2 cubes (150 × 150 × 150 mm^3) were tested for each hydration time (1, 7, and 28 days).

2.4.7. Environmental performance (EP)

The environmental performance, which can be defined as the ratio between CO_2 emissions by blends and the compressive strengths of the corresponding mortars [66], was calculated for the studied blends. The CO_2 emissions associated with each blend was determined considering the value of each component, f.i. 0.85, 0.0022 and 0.00 $kgCO_2eq./kg$ were taken for PC, limestone and gypsum, respectively [67], and 0.249 $kgCO_2/kg$ for calcined kaolinitic clay [68]. In addition, the European Federation of Concrete Admixture Associations (EFCA) have specified the CO_2 footprint of different admixtures [69]. A value of 0.689 $kgCO_2eq./kg$ has been assumed for the used SP [70] (Group B in the EFCA categorisation), and 0.73 $kgCO_2eq./kg$ for the C-S-H seeding admixture [71]. Consequently, the calculated CO_2 emissions per kilogram for all CCx-LC^3 blends, including admixtures (SP and C-S-H gel nucleation seeding where applicable), are 0.52 and 0.54 kg CO_2eq/kg for unseeded and seeded blends, respectively. For CC1-LC^3, the calculated CO_2 is marginally higher due to its higher SP content (0.53 kg CO_2eq/kg for the unseeded sample). For plain PC with SP, this value rises to 0.86 kg CO_2eq/kg.

2.4.8. Isothermal calorimetry of pastes

The heat released by all studied pastes was measured with the calorimeter described in Section 2.4.4. The pastes were placed in glass ampoules, with water used as the reference material [72]. Heat measurements were carried out over a 7-day period at 20 °C, excluding the first 45 min after mixing, which were required for thermal equilibrium.

2.4.9. Thermal analysis (TA) techniques (clays and pastes)

Thermogravimetric analysis of raw clays (milled down to $D_{v,50}$~11 μm and dried at 105 °C for 2 h) and LC^3-cement pastes (crushed, sieved between 2 and 4 mm and ground in an agate mortar for 10 min, without arresting hydration) was performed in an SDT-Q600 analyser (TA Instruments, New Castle, DE). Data were collected from RT to 1000 °C by heating at 10 °C/min. For the clays and prior to the measurements, an isothermal treatment was applied which was 105 °C for 30 min, i.e. within the TA chamber.

2.4.10. Mercury intrusion porosimetry (MIP)

The porosity study was performed with a Micromeritics AutoPore IV 9500 porosimeter (Micromeritics Instrument Corporation of Norcross, GA, USA), from 1 mm to 3.5 nm (pore entry radius) applying pressures 0–210 MPa in the step mode. A contact angle of 140° was assumed for calculations. For this study, pastes were crushed, sieved (the retained pieces ranged from 2 to 4 mm) and the water was arrested by immersion in isopropanol (20:1 of isopropanol:sample mass ratio) for 1 h to minimise alterations including carbonation [73]. After that, the pieces were kept in a stove at 40 °C until a constant weight.

3. Results and discussion

3.1. Characterisation of raw clays

The four low-grade kaolinite clays, i.e. RC1 to RC4, were numbered based on the heat released during calorimetry, as determined by the R^3-test at 7 days, see below. Additionally, two medium-grade clays were included, RC_{ref1} and RC_{ref2}, for comparison/reference purposes. All raw clays were characterised by XRF, LXRPD-RQPA and TA. Three analytical techniques were employed due to the significant errors involved in quantifying the kaolinite content in low-grade kaolinitic clays. These errors stem from the natural variability of clays including the possible pozzolanic performances of the amorphous fraction which is presently unknown. Table 2 presents the XRF data for all raw clays, including the Al_2O_3/SiO_2 ratios. As expected, the studied low-grade kaolinitic clays do not fully meet the empirical criteria outlined in Table 1. For instance,

Table 2
Elemental compositions, expressed as oxide wt%, for all studied clays from XRF data.[#]

	RC_{ref1}	RC_{ref2}	RC1	RC2	RC3	RC4
SiO_2	72.6(3)	76.6(3)	49.9(4)	63.4(4)	60.3(4)	63.3(4)
Al_2O_3	20.5(2)	14.8(2)	30.5(2)	16.5(2)	17.2(2)	16.6(2)
Fe_2O_3[a]	0.23(2)	0.18(1)	3.6(2)	5.9(2)	8.4(2)	6.1(2)
CaO	0.08(1)	0.06(1)	0.86(6)	1.25(8)	0.57(4)	0.96(7)
MgO	0.07(2)	0.08(2)	–	0.8(1)	2.0(2)	1.8(2)
SO_3	–	–	1.10(6)	0.11(1)	–	0.04(1)
Na_2O	–	–	0.55(6)	0.32(4)	0.11(4)	0.13(3)
K_2O	1.1(1)	1.3(1)	2.9(1)	3.4(2)	4.0(2)	4.1(2)
TiO_2	0.17(1)	0.14(1)	1.08(1)	0.75(1)	1.05(1)	0.71(1)
P_2O_5	–	–	0.42(2)	0.11(1)	–	0.04(1)
MnO	–	–	–	0.16(1)	–	0.04(1)
Others	0.03	0.03	0.14	0.04	0.06	0.03
Al_2O_3/SiO_2	0.28	0.19	0.61	0.26	0.29	0.26
LOI*	5.16	6.85	8.67	7.23	6.25	6.18

[#] Values in parentheses are the associated errors.
[a] Total Fe expressed as Fe_2O_3 weight percent.
* LOI: Loss on Ignition. Dried (105 °C for 2 h) and heated (950 °C for 2 h).

only RC1 shows an Al_2O_3 content greater than 18.0 wt%, and only RC1 exhibits an Al_2O_3/SiO_2 ratio above 0.30, although several other samples are close. Only RC1 and RC2 display loss on ignition (LOI) values exceeding 7.0 wt%. Concerning the reference clays, it is noteworthy that RC_{ref2} has an Al_2O_3 content lower than 18 wt%, i.e. ~15 wt%. The CaO content in all cases is low, see Table 2. Another important observation is that all studied raw clays contain significant amounts of Fe_2O_3 (≥3.5 wt %), whereas in both reference samples, the Fe_2O_3 content is below 0.5 wt%. The role of Fe_2O_3 content in the calcined clay with respect to the pozzolanic performances is presently unknown to the authors. All the studied clays contain K_2O (3–4 wt%), primarily from muscovite (and microcline), see below.

The LXRPD patterns of the four raw clays (measured without an internal standard using CuKα_1 radiation) are given in Fig. 1, with the main phase peaks indicated. Table 3 presents the mineralogical composition of all raw clays as determined by RQPA, where the ACn contents are also given. The crystal structure codes, viz. ICSD (Inorganic Crystal Structure Database) or AMCSD (American Mineralogist Crystal Structure Database), used for the quantitative study have been included. "Common clays" typically consist of a heterogeneous mixture of phyllosilicates and can be categorized by the type of layers present, i.e., 1 or 2 tetrahedral (silicate-based) and 1 octahedral (aluminate-based) layers, such as 1:1 in the kaolinite group [74] and 2:1 in muscovite [74] and pyrophyllite [75].

On the one hand, the reference clays have larger crystalline kaolinite contents, ~20 and ~17 wt% for RC_{ref1} and RC_{ref2}, respectively. Very importantly, these clays have low amounts of muscovite/mica, i.e. <6 wt%, and this could imply that the amorphous contents in these two samples, ~20 wt%, see Table 3, could be kaolinite-like. On the other hand, the four studied clays have low percentages of crystalline kaolinite (below 15 wt%). Very importantly, these clays have relatively high amounts of crystalline muscovite ranging from ~18 to ~28 wt%. We consider this a very important feature as this may suggest that the non-crystalline fractions are more illite-like due to argillization.

Fig. S1, given in Supplementary Information (S.I.), presents the TGA-DTG plots for the four clays studied. This analysis aids in understanding the calcination processes of these samples with varying compositions. As reported in the literature [77], the dehydroxylation of kaolinite occurs through an endothermic peak between ~530 and ~590 °C, while the dehydroxylation of muscovite, the most abundant crystalline phase in these clays, takes place between ~820 and ~920 °C. Finally, the dehydroxylation of pyrophyllite occurs between 650 and 850 °C [77]. Broader dehydroxylation ranges (400–650 °C for kaolinite, 700–900 °C for muscovite [17], and 500–900 °C for pyrophyllite [78]) are also reported in the literature. The dehydroxylation of these clays is occurring between 300 and at least 700 °C. The weight losses between 300 and 600 °C are explicitly reported in Fig. S1, together with the corresponding kaolinite contents assuming that these losses are only due to kaolinite. In the four cases, kaolinite contents lower than 30 wt% were estimated, setting the upper amount of kaolinite [79]. In this work, the endotherms associated with kaolinite dehydroxylation are centred at 500, 516, 473, and 490 °C for RC1, RC2, RC3, and RC4, respectively. Additionally, a broad endothermic peak observed at ~650 °C (specifically at 624, 648, 617, and 693 °C for RC1, RC2, RC3, and RC4, respectively) is likely associated with the dehydroxylation of muscovite. Due to the small sample size used by this technique (~30–40 mg), the kaolinite content was also estimated by thermal analysis based on the weight loss [17] of the studied clays in a furnace, using ~5.0 g of sample, over the temperature range of 300 to 600 °C. The corresponding estimated kaolinite contents (ranging from ~22 to ~35 wt%) for the four studied clays are

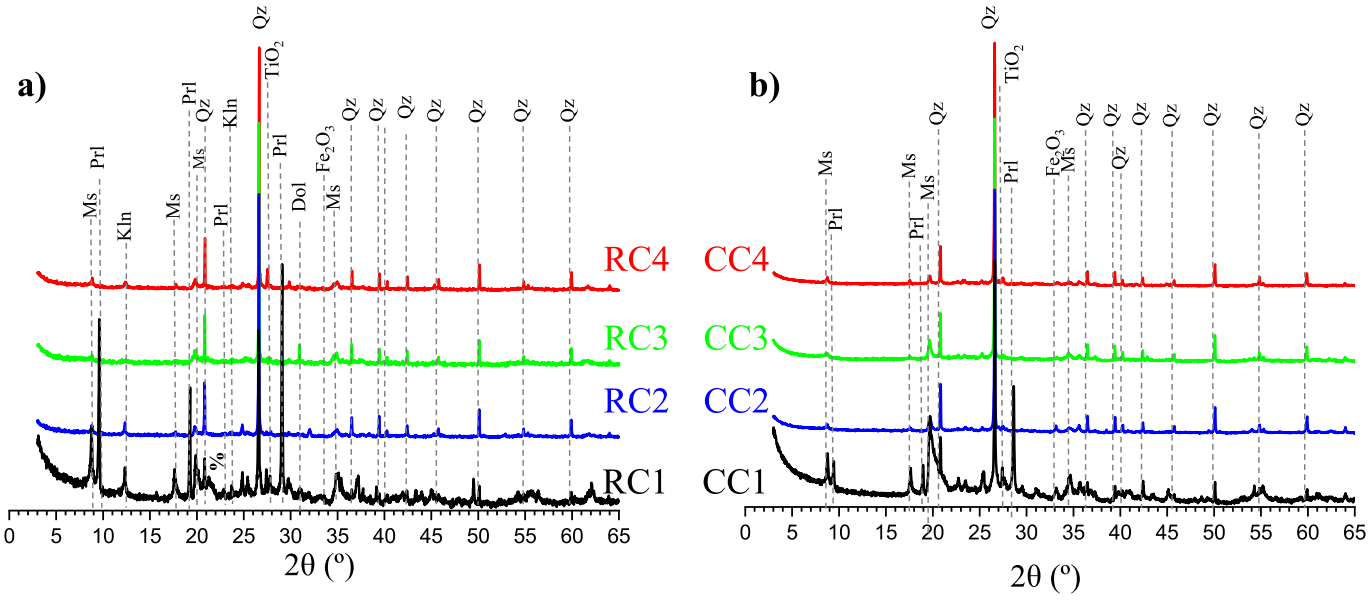

Fig. 1. CuKα_1 LXRPD patterns for (a) the raw clays (RC1, RC2, RC3 and RC4), and (b) calcined clays (CC1, CC2, CC3 and CC4), without internal standard. % stands for Goethite. The standard mineral abbreviations are used [76].

Table 3
RQPA results for all studied raw clays including ACn. Crystal structure codes of each mineral phase are included.[#]

wt%	RC_{ref1}[a]	RC_{ref2}[a]	RC1[a]	RC2[a]	RC3[b]	RC4[b]	Crystal structure code
Kaolinite	**20.3**(2)	**16.8**(2)	14.9(5)	8.8(3)	4.3(6)	12.0(5)	0020861[d]
Muscovite	5.7(3)	3.1(2)	**28.1**(3)	**23.9**(6)	**23.2**(7)	**17.7**(3)	0012229[d]
Fe_2O_3	0.3(1)	0.2(1)	–	–	–	–	88418[c]
Illite	–	–	–	–	1.0(1)	–	0005015[d]
Quartz	47.5(2)	53.6(2)	4.7(1)	36.8(1)	17.8(1)	30.3(1)	63532[c]
Pyrophyllite	–	–	12.0(3)	–	–	–	0010542[d]
Rutile	–	–	1.0(6)	0.5(1)	–	0.4(1)	64987[c]
Dolomite	–	–	–	–	0.6(1)	–	31277[c]
Microcline	4.4(3)	4.6(3)	1.7(2)	–	–	2.1(3)	0000194[d]
Anatase	0.6(1)	0.4(1)	–	–	–	–	9852[c]
Gibbsite	–	–	2.1(1)	–	–	–	001797[d]
Goethite	–	–	2.8(2)	–	–	–	0002226[d]
ACn	**21**	**21**	**33**	**30**	**53**	**38**	–

[#] Values in parentheses are the associated errors.
[a] $CuK\alpha_1$.
[b] $MoK\alpha_1$.
[c] ICSD.
[d] AMCSD.

given in Table 4, by assuming that the complete mass loss is due to kaolinite. Thus, Table 4 summarises the results of the estimated kaolinite contents obtained by XRF, RQPA, furnace analysis, and also provides the average of all these values. The kaolinite quantification by XRF is based on the assumption that all Al_2O_3 content which is not associated to a crystalline phase in Table 3 is within kaolinite.

3.2. Thermal activation and pozzolanic activity test

The choice of the calcination temperature was carried out based on operative reasons after an initial study. There is an industrial (brick) furnace operating at a maximum temperature of 860 °C, where large amounts of clays can be heated. This was considered essential as 100 kg of RC4 was heated to have material for concrete (and mortar) studies.

Thus, an initial TGA-DTG investigation of the raw materials was carried, see Fig. S1. 860 °C appears to be an appropriate calcination temperature, as it ensures complete dehydroxylation of all clays. In a second (necessary) study, the formation of new crystalline phases at this temperature was ruled out. The avoidance of recrystallization was determined by LXRPD, see Figs. 1 and S2 and Tables 3 and A2. Consequently, it was concluded that 860 °C was an adequate temperature (although not necessary the optimum for each sample). This was confirmed by the R^3 results, see below.

Table A1, in the annex, presents the XRF data for the calcined clays (CCx) and the reference samples. As expected, the LOI values are much lower than those of the raw clays, see Table 2, because of the decomposition of the hydrate phases. The textural properties of the milled calcined clays (particle sizes, specific surface area, and density) are presented in Table 5. The corresponding particle size distribution figures are shown in Fig. S3.

Table 4
Kaolinite contents from RQPA, thermal mass loss and XRF for all kaolinitic raw clays. The average values are calculated from the three approaches.

	RC_{ref1}	RC_{ref2}	RC1	RC2	RC3	RC4
RQPA /wt%	20.3	16.8	14.9	8.8	4.3	12.0
Furnace /wt%	44.7[$]	36.3[$]	31.4	35.5	26.8	21.9
XRF[*] /wt%	44.5	32.6	37.1	19.3	20.9	24.4
Average /wt%	37	29	28	21	17	19

[*] Obtained by considering all Al_2O_3 in kaolinite after subtracting the Al_2O_3 content in muscovite, microcline, pyrophyllite and gibbsite (determined by RQPA).
[$] TGA data.

3.2.1. LXRPD study of calcined clays

Table A2 presents the phase composition, including ACn, of the studied calcined clays and the reference samples. In all cases, kaolinite is either absent or present in very low amounts (i.e. 0.8 wt% for CC1), as expected. Additionally, when these results are compared with those of the raw clays in Table 3, the ACn contents have increased after calcination, as expected. The LXRPD patterns of the calcined clays, measured using $CuK\alpha_1$ radiation, are shown in Fig. 1b. It is important to highlight that no new phases were generated during the heating process, which could have otherwise reduced the pozzolanic activity of the calcined clays. The Rietveld refinement plots of the studied calcined clays, mixed with Al_2O_3 as an internal standard and measured using $MoK\alpha_1$ radiation, are shown in Fig. S2.

3.2.2. Pozzolanic activity of calcined clays by ASTM C1897-20

The pozzolanic activity of the calcined clays was tested following the ASTM C1897-20 standard (R^3-test) [34,80,81]. Fig. 2(a–b) shows the corresponding heat flow and cumulative curves up to 7 days for the calcined clays, including the references. On the one hand, the four samples studied exhibit a broad peak (see Fig. 2a), related to the pozzolanic reactions forming C-A-S-H gels and possibly ettringite [80]. The peak associated with CC1 is sharper, which may be partially associated with its higher Al_2O_3/SiO_2 ratio and lower Fe_2O_3 content.

The reference samples show significantly higher cumulative heat values at seven days, 539 and 457 J/g SCM for CC_{ref1} and CC_{ref2}, respectively. As detailed in the introduction, this would correspond to equivalent MK contents of 49 and 41 %. This is in line with its medium-grade kaolinite performances and it points out that the low Fe_2O_3 and muscovite contents enhanced the pozzolanic activity. On the one hand, low muscovite contents could indicate that the amorphous content in the pristine clay is more kaolinite-like. It is worth noting that the amorphous contents of CC_{ref1} and CC_{ref2} were ~42 wt%, see Table A2, suggesting that this fraction corresponds entirely to MK-like material. On the other hand, it has been reported [15] that the iron content plays a significant role in calcined kaolinitic clay pozzolanic performances; Fe_2O_3 contents of ~2.7 wt% were shown to enhance pozzolanic activity, which diminished by increasing Fe_2O_3 levels. This was justified by the deposition of iron oxides onto MK sheets as a gel in the calcination step. This gel acts as a screen between the MK particles and the aqueous solution, thereby hampering the pozzolanic reaction [15].

The four studied clays exhibit heat values ranging from 200 to 226 J/g calcined clay at 7 days, see Fig. 2b, indicating the low reactivity of these samples, consistent with [65]. The Fe_2O_3 content in the four studied samples is relatively high, 3.6, 5.7 8.4 and 6.1 wt% for RC1, RC2, RC3 an RC4, respectively. The Fe_2O_3 contents in the calcined clays are

Table 5
Textural properties of ball milled calcined clays (CCx). Reference data are included.[#]

	CC_{ref1}	CC_{ref2}	CC1	CC2	CC3	CC4
$D_{v,10}$ (μm)	2.6(1)	2.4(1)	2.0(1)	1.5(1)	1.1(1)	1.3(1)
$D_{v,50}$ (μm)	12.8(3)	11.6(2)	11.7(3)	12.0(3)	10.4(3)	9.2(1)
$D_{v,90}$ (μm)	48.3(9)	44.8(6)	78(4)	55(2)	56(2)	46(1)
SSA (m^2/g)	3.9(1)	3.6(1)	9.6(1)	4.5(1)	4.0(1)	18.4(1)
ρ (g/cm^3)	2.63(1)	2.61(1)	2.68(1)	2.71(1)	2.65(1)	2.69(1)

[#] Values in parentheses are the associated errors.

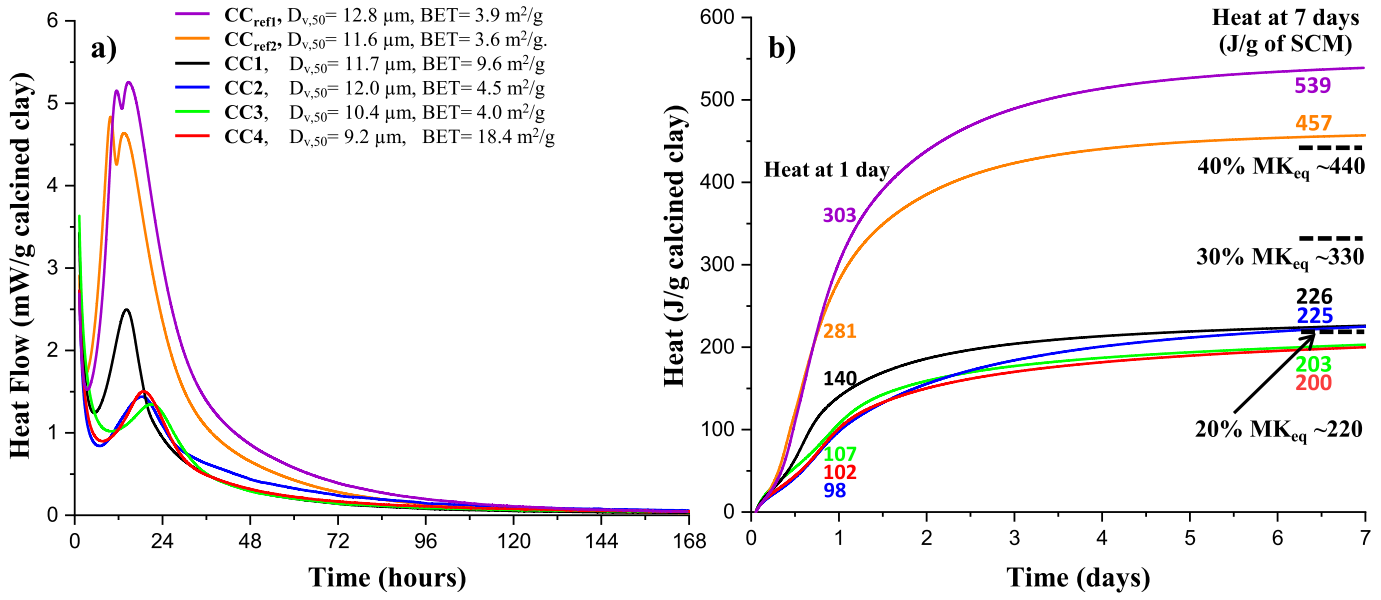

Fig. 2. (a) Heat flow and (b) cumulative heat curves of all milled CCx clays up to 7 days, including references. The heat released at 1 and 7 days is shown as inset.

totally consistent, see Table A1. Moreover, the high content of muscovite in RC1-RC4 indicates that the amorphous content cannot be equated to kaolinite.

Therefore, it is concluded that the amorphous content of ~42 wt% of CC_{ref1} and CC_{ref2}, see Table A2, is MK, but the amorphous contents of ~48, ~44, ~48 and ~45, for the CCx, are not completely MK but mixture of MK and other (less reactive) amorphous clays, like meta-illite. This is consistent with the bound water determination at seven days following ASTM C1897, see Table 6. CC_{ref1} and CC_{ref2} showed higher BW values, i.e. 9.7 and 8.0, respectively, in agreement with their medium pozzolanic activities [65]. It is noted that pure MK was reported to yield a BW value of 16.9 % [36]. Therefore, there is a relatively good agreement, 50 % of equivalent MK should yield ~8.5 % of BW. The quantitative agreement in the expected BW for CC1-CC4 is not that good, as 20 % of 16.9 should give 3.4 % and the measured BW values ranged from 4.3 to 5.7 %.

Considering both the cumulative heat release and the bound water values, following ASTM C1897 standard, it can be concluded that RC1 to RC4 are low-grade kaolinitic clays exhibiting relatively low pozzolanic activity, see Fig. 2 and Table 6. The next step is to investigate the impact of these low-grade calcined kaolinitic clays in the resulting LC^3-50 mortars. As CC_{ref2} showed pozzolanic features typical of medium grade kaolinitic clay with relatively low kaolinitic content, it was chosen as the reference for the remaining studies, i.e. LC^3-50 mortars and pastes.

Table 6
R^3-test key results, bound water (BW_{exp}) content and heat released, for the studied pastes at 7 days. The values of the reference calcined clays are also given for the sake of comparison.

	CC_{ref1}	CC_{ref2}	CC1	CC2	CC3	CC4
BW_{exp} (%)	9.7	8.0	5.5	5.4	5.7	4.3
Heat (J/g of CC)	539	457	226	225	203	200

3.3. LC^3 mortars

3.3.1. Flowability of mortars: slump and slump retention

LC^3-type mortars were produced as outlined in Section 2.3. The quantities of SP needed to attain an initial self-flow of 200 ± 20 mm are given in Table 7 for each mortar. Additionally, to control slump retention, flow measurements were performed at 30 and 60 min after mixing (t_{30} and t_{60}, respectively). The corresponding values for the PC-525 and CC_{ref2}-LC^3 mortars are also provided for comparative purposes.

A general drawback of LC^3 mortars is their slump retention, particularly for high-grade kaolinitic clays or clays with a high specific surface area. Based on prior studies [47,49,59], a polycarboxylate-based SP specifically designed to enhance slump retention was used. This SP is based on an "intelligent cluster system" [82], which releases some PCE for initial dispersion and gradually releases the remaining amount

Table 7
Slump retention study of all CCx-LC^3 mortars, prepared with SP and w/b = 0.40. PC-525 and CC_{ref2}-LC^3-SP mortars are included as references.[#]

Mortars	SP (wt%)	Slump t_0 (mm)	Slump t_{30} (mm)	Slump t_{60} (mm)
PC-525-SP	1.20	190(1)	264(1)	288(1)
CC_{ref2}-LC^3-SP	0.50	210(1)	267(1)	276(1)
CC1-LC^3-SP	1.25	198(1)	190(2)	146(1)
CC2-LC^3-SP	0.60	219(4)	229(3)	207(2)
CC3-LC^3-SP	0.90	208(1)	198(1)	173(1)
CC4-LC^3-SP	0.70	202(1)	206(1)	192(3)

[#] Values in parentheses are the associated errors.

during the hydration process to mitigate slump retention issues. The same SP and processing procedure were applied for all mortars. Therefore, it is noteworthy that CC_{ref2} mortar, which has the highest MK content, requires the lowest SP amount. This observation, plus the wide range of SP dosages required across the CC1-CC4 mortar series, suggests that MK content is not the primary factor governing SP demand. Moreover, the SSA is not either the main parameter as CC4 exhibits the highest SSA value but its SP requirement is relatively modest, see Table 7. We speculate that CC1-LC^3 mortar required the largest amount of SP because the calcined clay contained ~18 wt% of pyrophyllite, a 2:1 clay. This is consistent with findings that show a reduction in slump flow diameter in self-compacting concrete with increasing substitution of PC by calcined pyrophyllite (at 750 °C) [83]. However, more research is needed to test this assumption. Regarding the SP demand of CC2 to CC4, the Fe_2O_3 content emerges as a relevant factor, indicating that calcined clays with higher iron contents generally require increased SP dosages. This is in line with a previous publication [20], but it also requires further investigations.

Concerning the possible slump loss, the data shown in Table 7 indicate that this is not a problem for the employed SP. Only CC1-LC^3 mortar displayed a minor but significant slump loss at 1 h. To end this subsection, it is important to highlight that the same SP dosage, determined for the unseeded mortars, was employed in the preparation of mortars containing the STE53 admixture.

3.3.2. Compressive mechanical strengths

The compressive strength values for the studied mortars at 1, 7, and 28 days are presented in Fig. 3. For comparison, the corresponding values for mortars prepared with CC_{ref2} and plain PC-525 are also included. For the unseeded LC^3 mortars, compressive strengths ranged from 11 MPa (for CC1-, CC2-, and CC4-LC^3-SP) to ~16 MPa for CC3-LC^3 at ~1 day, and from ~42 MPa (for CC1-LC^3-SP) to ~51 MPa (for CC3-LC^3-SP) at 28 days. It is worth noting that RC3 was the clay with the highest amorphous content that it may have faster initial pozzolanic reaction kinetics. These values are relatively low compared to those obtained for the PC-525 mortar, which is undoubtedly due to the lower reactivity of the calcined low-grade kaolinitic clay (see Table 6).

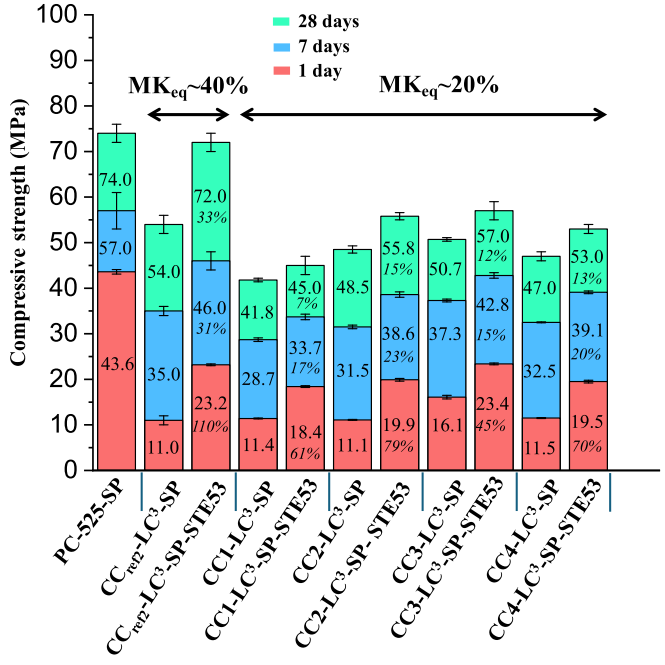

Fig. 3. Compressive strengths for all unseeded and seeded (STE53) CCx-LC^3 mortars at 1, 7 and 28 days. Data for plain PC-525-SP and CC_{ref2}-LC^3-SP are also included as references. The percentage increase relative to the mortars without the strength-enhancing admixture, at a given age, is also shown (*in italics*).

Notably, when C-S-H gel nucleation seeding was employed, the compressive strength values measured at 1 day markedly increased. The strengths at 1 day for CC1 to CC4 ranged from ~18 to ~23 MPa, reflecting an improvement of 45 % to 79 %. Moreover, the compressive strengths of the seeded LC^3 mortars continued to increase during hydration at 7 and 28 days compared to the unseeded mortars, although at a slower rate, ranging 45 to 57 MPa at 28 days.

It is important to emphasize that CC_{ref2}-LC^3 mortar, which has double MK content, ~40 wt%, also developed 11 MPa at 1 day. This shows that although pozzolanic reaction may take place, see below, the contribution to impingement/connectivity of the solid particles is not very significant. However, C-S-H gel nucleation seeding boosted this by strength at 1 day by 110 %, see Fig. 3. By using C-S-H gel nucleation seeding, this calcined medium-grade kaolinitic clay, i.e. CC_{ref2}, yields a mortar with the same strength at 28 days than that of neat PC-525, 72 and 74 MPa, respectively. Finally, two remarks can be made. Firstly, and as expected, it is clear from Fig. 3 that MK content plays the key role from seven days onwards. The CC_{ref2}-LC^3 mortar, with the highest MK content, exhibits superior performance at 7 and especially at 28 days (in both unseeded and seeded specimens), due to an increased contribution from pozzolanic reactions. Secondly, it is underlined that CC3 displayed relatively low heat, i.e. 203 J/g, but it shows the largest compressive strength within this low-grade kaolinitic clay series. Interestingly, this calcined clay showed the fastest heat development in the R^3 test in the 0–6 h interval, see Fig. 2b. We speculate, based on this and other unpublished observations, that SCMs which display the fastest growth in the R^3 heat plot, in the 0–6 h region, usually yield comparatively largest mechanical strength. However, more investigations are needed to determine if this singular observation results in a general trend.

3.3.3. Environmental performance (EP)

The EP indicator is defined as the ratio between CO_2 emissions of the blends and the compressive strength of the corresponding mortars [66]; thus, the lower the EP values, the system becomes more environmentally sustainable. The EP values for all the studied LC^3 mortars, including CC_{ref2} and plain PC-525, at 1 and 28 days of hydration are presented in Fig. 4. Compressive strength values are also included for better comparison.

At 1 day, see Fig. 4a, the LC^3-50 mortars exhibit much higher EP values, i.e. ~47 gCO_2/MPa, (indicating worse performance) than plain PC-525, which shows 20 gCO_2/MPa, due to the (much) lower mechanical strengths of the LC^3 mortars. Only, CC3-LC^3 mortar has an intermediate EP value, ~33 gCO_2/MPa, because its high compressive strength at one day. However, when the LC^3 mortars are seeded, the differences with PC-525 decrease significantly, particularly for seeded CC3- and CC_{ref2}-LC^3-SP-STE53 mortars, with values ~23 gCO_2/MPa.

As hydration time increases, EP values decrease significantly due to the corresponding increase in compressive strength for the same CO_2 emissions. At 28 days, see Fig. 4b, EP values for LC^3 mortars prepared with CC2, CC3, and CC4 (10.7, 10.3, and 11.1 gCO_2/MPa for unseeded samples, respectively, and 9.6, 9.4, and 10.1 gCO_2/MPa for the seeded samples, respectively) are lower than that of PC-525 (11.6 gCO_2/MPa). For CC1, the EP values are worse, ~12 gCO_2/MPa, due to the lower compressive strengths. For reference CC_{ref2}-LC,[3] the EP values are significantly lower (9.6 and 7.4 gCO_2/MPa for unseeded and seeded samples, respectively, due to the combination of low emissions and competitive compressive strengths. Notably, the EP value of the seeded CC_{ref2}-LC^3 is comparable to that of an unseeded LC^3-50 (7.2 gCO_2/MPa) binder prepared with a high-grade (~74 wt%) calcined kaolinite clay, following the same procedure [59] and the same w/b ratio (0.40). Finally, it is worth pointing out that these EP estimations do not take transport emissions into account. If medium-grade kaolinitic clays are not locally available, the CO_2 emissions from transportation may increase the overall EP, making locally available low-grade kaolinitic clays a more favourable option.

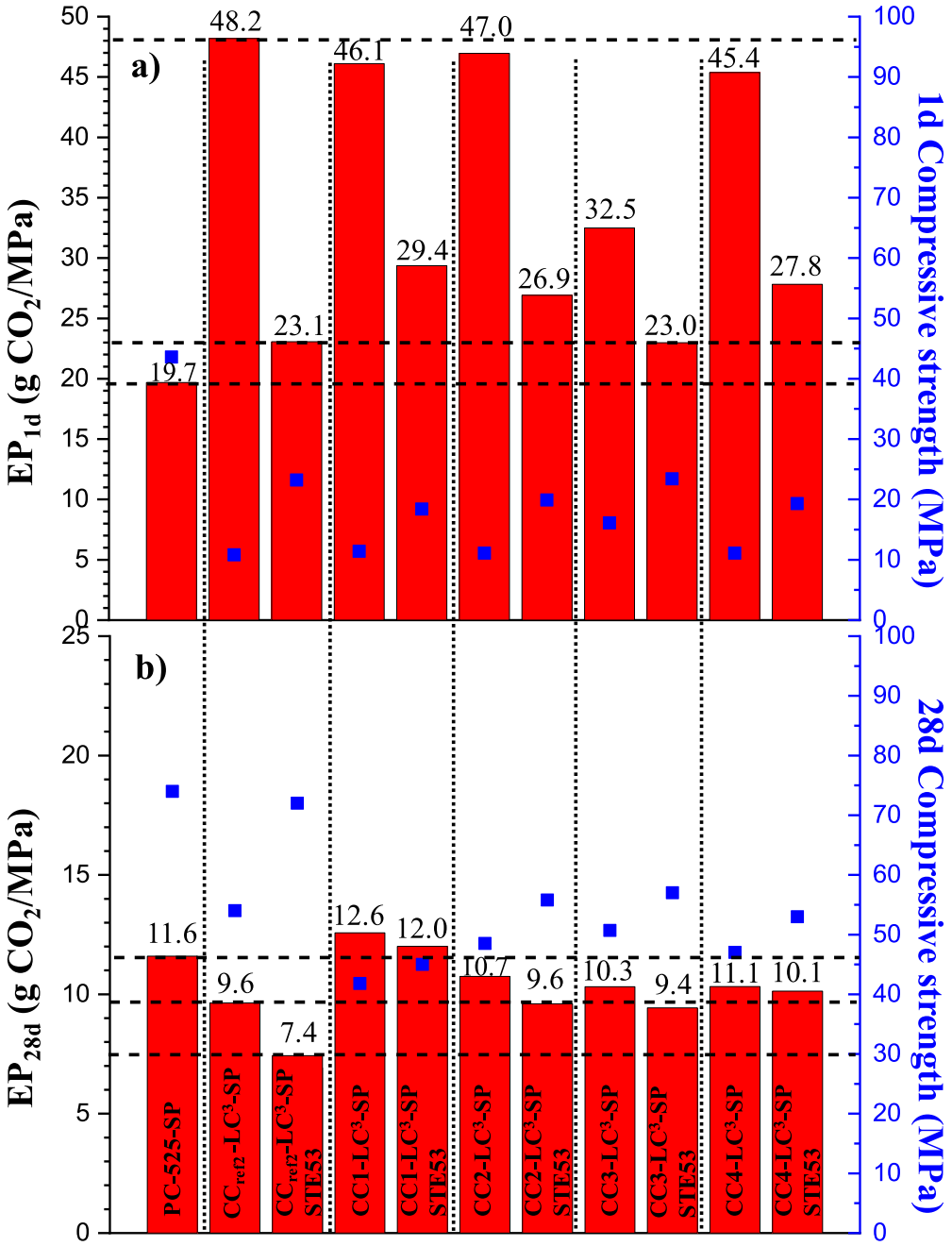

Fig. 4. Environmental Performance values, in g of CO_2/MPa, referred to 1 kg of binder, at (a) 1 day and (b) 28 days for all mortars. PC-525-SP, CC_{ref2}-LC^3-SP and CC_{ref2}-LC^3-SP-STE53 are shown for the sake of comparison. Mechanical strengths are also displayed on the right axis.

3.4. LC^3 pastes

3.4.1. Calorimetry

Fig. 5(a–d) presents the calorimetric data for the pastes without (Fig. 5a–b) and with (Fig. 5c–d) STE53. In Fig. 5a and c, the heat flow traces are shown for the first 80 h, for better visualisation of the early-age reactions. The first heat flow peak, located close to 9 h for the LC^3-pastes, is mainly due to C_3S hydration and its integrated area decreases because of the 50 % dilution. The hydration reaction takes place at earlier hydration times due to the filler effect [51–53,84]. All LC^3 pastes showed similar values, with slightly higher heat flow values recorded for CC4-LC^3-SP, the calcined clay of which has the smallest particle size distribution and the highest SSA. Fig. 5a also shows that the main alite peak takes place at ~16 h for neat PC-525-SP. This is delayed with respect to the paste without SP, ~10 h not shown, and it is undoubtedly due to the addition of the SP. The second peak, located close to 40 h for the LC^3-pastes, see Fig. 5a, is associated with the aluminate reaction, which is due to the clinker phases, i.e. C_3A and C_4AF, but it also contains a calcined clay contribution from the Al in MK [8,48,85]. The position of the aluminate peak has been documented to strongly vary depending on the gypsum concentration in the binder [84]. The 3 wt% gypsum addition seems to be too high, for pastes with these calcined low-grade kaolinitic clays. Calcium sulfate optimisation was not within the scope of this initial work.

The use of the C-S-H gel nucleation seeding admixture has some important consequences as shown in Fig. 5c: (i) it reduced the duration of the induction periods, as indicated by the vertical purple lines, with times ranging from 2.0 to 2.7 h for unseeded LC^3-pastes and from 1.1 to 2.2 h for seeded pastes; (ii) it moderately increased the height of the alite hydration peak, as indicated by the horizontal light blue lines; and (iii) it

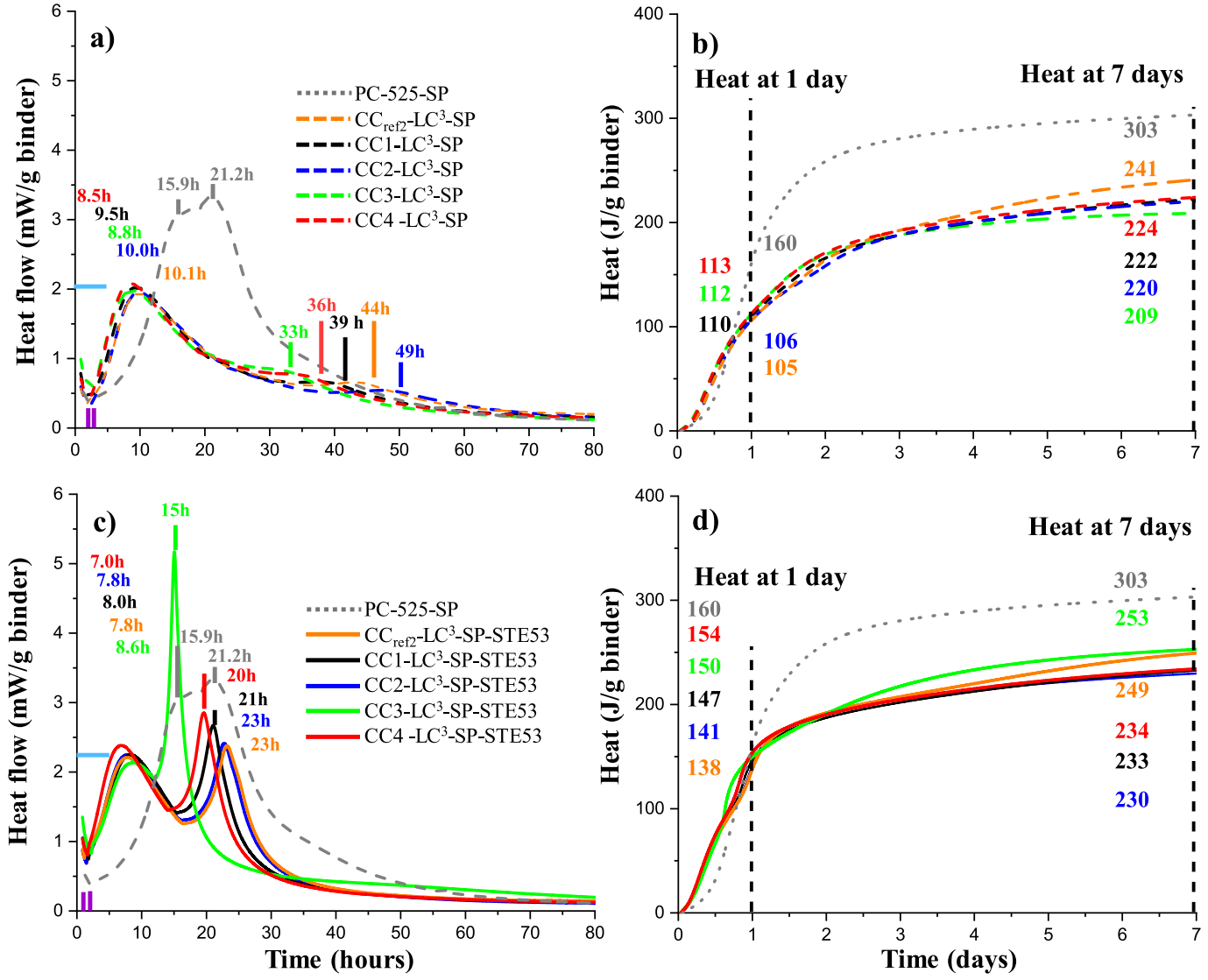

Fig. 5. Heat flow (a) and (c), and cumulative heat (b) and (d) curves for the CCx-LC^3 pastes. Results for the unseeded pastes are shown in (a) and (b). The results for the seeded pastes are shown in (c) and (d). CC$_{ref2}$-LC^3 and PC-525 curves are also included for comparison. Numbers inside indicate the times for the main signals in (a) and (c); the heats evolved at 1 day and 7 days are displayed in (b) and (d).

significantly increases and sharpen the aluminate hydration peaks. This third effect is particularly conspicuous for CC3-LC^3, where the aluminate peak takes place at 15 h. It is noted that this clay has the highest iron content, therefore it is not surprising that the aluminate peak has a contribution from iron species hydration. This is evidenced by the observation that CC4, which has the second highest iron content, see Table 2, showed the peak at 20 h, the fastest after CC3. However, more parameters should play a role, like MK content and SSA, as CC2 has a relatively high iron content but the trace of its aluminate peak is very similar to that of CC$_{ref2}$, a clay with very little Fe_2O_3 content. In any case, the alkanolamine content within the accelerator admixture is promoting iron-containing species hydration. These results are fully consistent with previous studies [8,47,49].

Fig. 5b–d shows the cumulative heats. Several observations can be made. Firstly, the LC^3 pastes exhibit greater heat releases than those expected from the dilution effect. Neat PC paste released 303 J at seven days. If the heat is coming only from the hydration of PC, then ~158 J/g would be expected, i.e. 303 × 0.52. However, the pastes without accelerating admixtures developed heats from 210 to 240 J/g. Therefore, there is a contribution from the pozzolanic reactions. This simple calculation cannot be done at 1 day due to the enhanced alite hydration resulting from the filler effect. Secondly, it is worth pointing out that CC$_{ref2}$ has double MK content but it starts to differentiate at 3 days and later. This suggests that early age reactivity of MK, between 12 h and 3 days is mainly governed not by the amount of MK but rather by other features which are not known at the time of writing. Intrinsic disorder and SSA of MK are possible candidates. However, the determination of phase-dependent textural and disorder properties is very challenging. In any case, this observation is fully in line with the relatively lower mechanical strengths of CC$_{ref2}$-LC^3 mortars at one day but ramping up at seven days, see Fig. 3. Thirdly, there is a clear cumulative heat increase at 1 day for the strength-enhancing admixture-containing pastes. This enhancement is primarily due to the boosted aluminium/iron hydration peak, previously discussed. Fourthly, the increase in heat release for CC3-LC^3-SP-STE53 due to the admixture is substantial in the period 3 to 7 day, see Fig. 5d. This is in addition to the peak observed at 15 h and it points towards iron activation due to the admixture.

To end this subsection, it is detailed how the amount of gypsum was selected. It is explicitly stated that the amount of gypsum has not been optimised here. The optimisation of the sulfate content is a complex matter subjected to choices. Even if the early-age compressive strength is chosen as the figure-of-merit to optimise, the curing time must be

decided as well as the addition (or not) of admixtures. A very recent paper [86] carried out a thorough optimisation based on compressive strength at two days (typical of cement producers), for mortars prepared with w/b = 0.50 and without the use of superplasticiser. We have a related ongoing investigation but based on compressive strengths at one day (typical of concrete producers), for mortars prepared with w/b = 0.40 and using admixtures (superplasticiser and strength-enhancing). The output of this investigation will be reported elsewhere. The choice of the 3 wt% gypsum content was the result of two constraints: (i) to have the same sulfate content in the four binders for comparative studies, and (ii) the selected amount must not lead to undersulfated conditions, i.e. to have the aluminate peak on top of the alite peak. Hence, a preliminary calorimetric study was carried out for the amount of SP determined by the slump and for 2 wt% of STE53 admixture. In these conditions, for the LC^3 blend based on CC3 and 3 wt% of gypsum, the alite peak took place at 9 h and the aluminate peak took place at 15 h, see Fig. 5c. This 6 h difference between the two key processes was judged acceptable and this gypsum content was selected.

3.4.2. *Phase assemblage of all pastes (RQPA and TA)*

Both unseeded and seeded pastes were prepared according to the procedures outlined in the experimental section for TA and LXRPD analysis. The pastes were just gently ground for 10 min without and with 20 wt% of Al_2O_3 for TA and LXRPD, respectively. As the hydration process was not halted by solvent exchange, the amorphous content determined by RQPA (ACn_T) includes both the amorphous/non-crystalline phases and the free water. However, some water is also lost during the grinding process, this fraction was determined by TA as described in [59].

The thermal analysis study aims to quantify: (i) the water loss during the grinding process, which is needed to refer the RQPA results to 100 g of fresh paste, (ii) the amounts of portlandite (CH), and the amount of $CaCO_3$ (Cc). For proper comparisons, all results are based on 100 g of fresh paste, i.e. nominal water content. Fig. 6a–d displays the thermogravimetric (TGA) traces for the four studied LC^3 pastes, also showing in the insets the amounts of CH and Cc, as determined from the weight losses and referred to the fresh pastes. Table S2 provides the weight loss values obtained from TA for the four pastes in two temperature ranges, i.e. from RT to 550 °C and from 550 to 900 °C. The weight loss measured from RT to 550 °C was attributed to H_2O, while the weight loss from 550 to 900 °C was considered as CO_2.

Table 8 presents the percentages of CH and Cc obtained from the TA data. Portlandite contents have been determined using the tangential method [87]. Cc contents are determined based on the overall weight loss between 550 and 900 °C. As the Cc content in the PC is 5.0 wt% and is diluted to 52 %, the Cc content of the four LC^3 binders is 17.6 wt% when expressed in relation to the dry binder or 12.7 wt% when referred to the fresh pastes. The theoretical weight losses should be 5.5 % but the

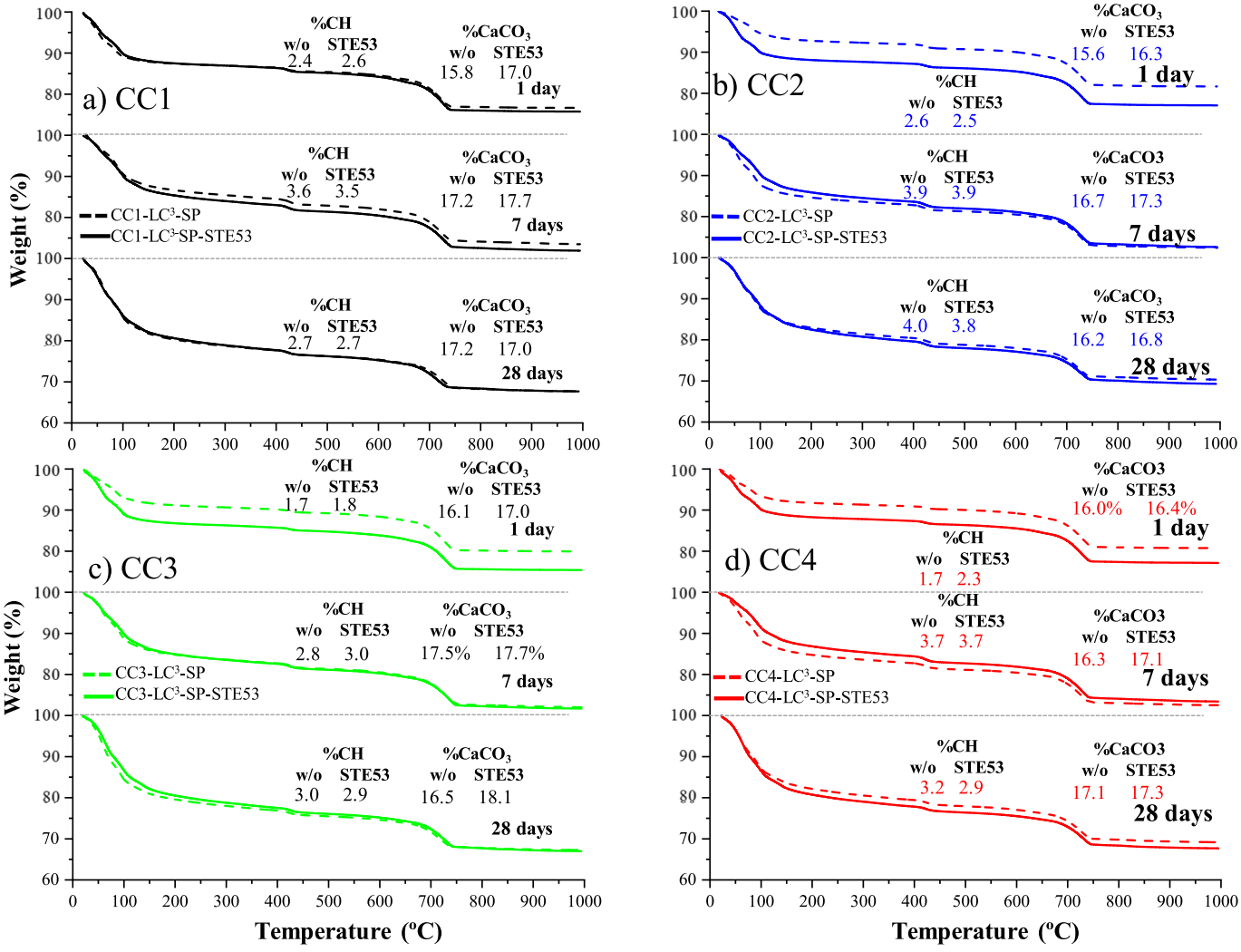

Fig. 6. Thermal analysis curves for the four CCx-LC^3-SP pastes at 1, 7 and 28 days. Unseeded specimens (dashed lines), seeded specimens (solid lines). The weight loss associated to portlandite, calculated by the tangent method, are referred to 100 g of fresh paste. w/o stands for without.

Table 8
Calcium carbonate and calcium hydroxide contents, referred to 100 of fresh paste, as measured by thermal analysis and Rietveld quantitative phase analysis. CH_{calc} contents are calculated from C_3A, C_4AF and C_3S degrees of hydration (Eqs. (1)–(3)). CH_{pozz} is the estimation of portlandite consumption in the pozzolanic reactions and the values are calculated by subtracting CH_{RQPA} from CH_{calc}. DoR MK has been obtained from Eqs. (4) and (5).

	Time (d)	$CaCO_{3\ TA}$	$CaCO_{3\ RQPA}$	CH_{TA}	CH_{RQPA}	CH_{calc}	CH_{pozz}	DoR MK (%)
	1	15.8	13.2	2.4	2.3	5.3	3.0	40–43
CC1-LC^3-SP	7	17.2	11.5	3.6	3.9	6.9	3.0	41–44
	28	17.2	11.3	2.7	3.6	7.3	3.7	49–53
	1	17.0	11.5	2.6	3.3	5.4	2.1	28–30
CC1-LC^3-SP-STE53	7	17.7	11.2	3.5	3.7	6.8	3.1	42–45
	28	17.0	10.2	2.7	3.4	7.2	3.8	51–55
	1	15.6	12.7	2.6	2.4	4.6	2.2	30–32
CC2-LC^3-SP	7	16.7	11.1	3.9	3.7	7.1	3.4	45–49
	28	16.2	10.7	4.0	3.9	7.2	3.3	45–48
	1	16.3	10.3	2.5	2.8	5.1	2.1	31–33
CC2-LC^3-SP-STE53	7	17.3	10.9	3.9	3.9	7.0	3.2	41–45
	28	16.8	10.4	3.8	3.5	7.3	3.8	51–54
	1	16.1	12.6	1.7	2.1	5.1	3.0	45–48
CC3-LC^3-SP	7	17.5	11.2	2.8	3.0	7.0	4.0	60–65
	28	16.5	11.4	3.0	3.4	7.2	3.8	57–62
	1	17.0	11.6	1.8	2.8	5.1	2.3	35–37
CC3-LC^3-SP-STE53	7	17.7	10.3	3.0	3.2	6.9	3.7	56–60
	28	18.1	10.6	2.9	3.0	7.2	4.2	63–68
	1	16.0	11.9	1.7	2.9	5.1	2.2	34–37
CC4-LC^3-SP	7	16.3	12.0	3.7	3.9	7.1	3.2	48–52
	28	17.1	11.1	3.2	3.6	7.3	3.7	56–60
	1	16.4	12.8	2.3	2.8	5.2	2.4	37–40
CC4-LC^3-SP-STE53	7	17.1	10.4	3.7	3.4	6.9	3.5	54–58
	28	17.3	10.0	2.9	3.6	7.2	3.6	56–60

The amount of $CaCO_3$ in the fresh paste is 12.7 wt%, which should slightly decrease over time due to carboaluminate formation. $CaCO_3$ contents can also increase because accidental carbonation.

measured values are larger, ranging 7.5–9.2 %, see Table S2. This leads to high Cc contents ranging 15.5–17.7 wt% (referred to 100 g of fresh paste). The obtained Cc values are 3 to 5 wt% higher due to two factors: (i) partial carbonation, and (ii) there is a H_2O loss contribution between 550 and 900 °C. Conversely, the Cc contents determined from RQPA, see just below, also reported in Table 8, are much smaller, i.e. ~11 wt%. This indicates that the sample preparation and data acquisition for the LXRPD study did not lead to additional crystalline calcium carbonate.

The Rietveld plots based on the LXRPD patterns for the studied LC^3 pastes (unseeded and seeded) are displayed in Fig. S4. Tables A3–A6 show the complete phase assemblage from RQPA (MoKα_1 radiation) based on 100 g of fresh paste at the three studied ages. In these tables ACn_T represents the combination of the amorphous content (ACn) determined by RQPA, using the internal-standard methodology, plus the small amount of water released during the grinding procedure and determined by TA. Here, it is assumed that the water losses during the 10 min grinding, for the two sample preparations, are the same.

The RQPA results of the pastes, Tables A3–A6, provide valuable information that can be grouped into two principal categories: the reaction (i.e. disappearance) of the anhydrous phases and the formation of hydrated products. Regarding the behaviour of the anhydrous cement phases, the degree of hydration (DoH) values of the phases with relatively fast kinetics (C_3S, C_4AF, and C_3A) are shown in Table 9. Five key observations can be made concerning the anhydrous phase evolution.

i) The degree of hydration (DoH) of C_3S in LC^3 pastes is higher than 95 % at 7 days and ~100 % at 28 days. At 1 day, C_3S DoH ranged 65–75 %. Concerning the admixture effect in C_3S hydration, its DoH is slightly accelerated at one day. There are no relevant differences at 7 and 28 days.
ii) The reactivity of C_4AF, see Table 9, is faster in the STE53 containing pastes. This in agreement with previous findings [8,48,49] and it is likely attributable to the combination of higher surface because the C-S-H gel nucleation seeding and the alkanolamine content of the STE53 admixture.

Table 9
Degree of hydration (DoH) of C_3S, C_4AF and C_3A for the four pastes at the studied hydration ages.

		DoH C_3S (%)	DoH C_3A (%)	DoH C_4AF (%)
CC1-LC^3-SP	1d	73.8	75.0	84.2
	7d	95.0	100.0	89.5
	28d	100.0	100.0	100.0
CC1-LC^3-SP-STE53	1d	75.7	87.5	92.1
	7d	95.0	100.0	100.0
	28d	100.0	100.0	100.0
CC2-LC^3-SP	1d	64.4	81.3	81.6
	7d	97.0	100.0	89.5
	28d	100.0	100.0	100.0
CC2-LC^3-SP-STE53	1d	71.3	68.8	89.5
	7d	95.5	100.0	89.5
	28d	100.0	100.0	100.0
CC3-LC^3-SP	1d	70.8	87.5	78.9
	7d	96.5	100.0	92.1
	28d	100.0	100.0	100.0
CC3-LC^3-SP-STE53	1d	72.3	100.0	92.1
	7d	96.0	100.0	97.4
	28d	100.0	100.0	100.0
CC4-LC^3-SP	1d	71.3	68.8	84.2
	7d	97.0	100.0	89.5
	28d	100.0	100.0	100.0
CC4-LC^3-SP-STE53	1d	72.8	81.3	86.8
	7d	95.5	100.0	97.4
	28d	100.0	100.0	100.0

iii) The amount of Cc measured by RQPA, see Table 8, is consistent with the expected values, slightly lower than 12.7 wt% because of carboaluminate formation. Moreover, the Cc contents in the STE53 containing pastes are slightly lower than those determined for the pastes without the admixtures. This is probably due to the carboaluminate enhanced formation in the presence of the admixture because Al^{3+} and Fe^{3+} mobilisation. These observations also rule out significant carbonation in the powder diffraction study.
iv) C_3A reacts completely before 7 days of hydration.

v) Belite hydration could start at 28 days but the scattering of the result and the low content of belite do not allow for conclusive results, see Tables A3–A6.

Concerning the quantification of hydrated phases, the following observations can be noted:

i) The measured amounts of ettringite (AFt), see Tables A3–A6, are quite low (1.0–2.5 wt%) despite the fact that hydration was not arrested by solvent exchange. The maximum amount of AFt would be 12.6 wt% considering SO_3 as the limiting reactant. Lower amounts of AFt, 8–10 wt%, are usually measured in LC^3-50 systems because the sulfate adsorption in C-(A)-S-H gel [88] and experimental inaccuracies. The low values found in our study point towards partial AFt decomposition in the sample conditioning procedure, i.e. 10 min grinding to have homogeneous dispersion of the internal standard in the specimens to be measured. The 'mix and measure' approach is being developed to solve this problem [89,90], i.e. avoiding sample conditioning is critical to accurately measure labile phases.
ii) As expected, hemi- and mono-carboaluminates (Hc and Mc, respectively) were not observed at one day but measured and quantified at 7 and 28 days. STE53 admixture enhances the carboaluminate formation, which is more evident at 28 days. The (Hc + Mc) contents at 28 days were 0.7, 0.7, 0.9 and 0.9 wt% for CC1, CC2, CC3 and CC4, respectively. The corresponding values for the pastes with STE53 were 1.2, 1.2, 1.1 and 1.1 wt%. However, these values do not fully justify the enhanced dissolution/reactivity of calcite discussed previously. We speculate that a significant fraction of carboaluminates and even carboferrates could be amorphous. Tailored research is needed to address the crystallinity nature of carboaluminates.
iii) To end this subsection, we address the portlandite determination as it is an indirect way to investigate the pozzolanic reactions. The analysis is centred on the values determined from RQPA because the amounts of crystalline $CaCO_3$ were in line with the expected values. However, portlandite can be partly carbonated to yield amorphous calcium carbonate that would not be detected in this powder diffraction study. The CH_{pozz} values, see Table 8, are the estimated $Ca(OH)_2$ amounts consumed in the pozzolanic reactions. These numbers should be considered as maximum values as the procedure neglects any possible carbonation.

In order to estimate the degree or reaction (DoR) of MK in the pastes, some calculations have to be carried out. Firstly, the MK content of the calcined clays was close to 20 wt% as detailed in Section 3.2.2. Due to the fact that the calcined clay was dosed at 30 wt% and diluted with w/b = 0.40, the MK contents in the fresh pastes are 4.3 wt%. Secondly, the CH contents obtained from the hydration of the clinker phases, i.e. CH_{calc}, have been determined by mass balance calculations as schematically shown in Fig. 7. The stoichiometries of the chemical reactions are given in Table A7. C_4AF hydration is considered to yield: (i) the iron within iron-siliceous hydrogarnet; and (ii) the aluminium within ettringite at 1 day, and within Hc at 7 and 28 days. Thirdly, the CH consumed in the pozzolanic reaction, CH_{pozz}, are also given in Table 8 and calculated by subtraction, i.e. CH_{calc}-CH_{RQPA}. As expected, the CH_{pozz} values increase with the hydration time and they ranged 2.1–3.0 wt% at 1 d and 3.3–4.2 wt% at 28 days. Finally, the MK DoR values were estimated from the pozzolanic reactions also given in Table 8. A range is provided because the pozzolanic reaction between MK and CH could yield, in addition of C-(A)-S-H, Hc or Mc. It is noted that the CH consumption (slightly) depends upon the formed carboaluminate phase, see Table A7. The MK degree of reaction is estimated to be 30–45 % at 1 day which increased to 50–70 % at 28 days. Therefore, even for the employed calcined low-grade kaolinite clays, more than 30 % of the MK is unreacted at 28 days, and hence available for further pozzolanic reaction if species diffusion can take place.

3.4.3. *MIP of LC^3 pastes*

The MIP cumulative porosity curves for the studied LC^3 pastes (both unseeded and seeded) at two hydration times (1 and 28 days) are shown in Fig. 8a–d. The cumulative porosity values at one day of hydration are significantly lower in the STE53 containing pastes. This is aligned with: (i) the improved mechanical strength reported in Fig. 3; and (ii) the enhanced DoH of C_4AF and also of C_3S. At 28 days, seeded pastes display slightly lower porosities but the differences are much less pronounced. This is also in line with the improved mechanical strength performances at 28 days which are quantitatively lower than those measured at one day.

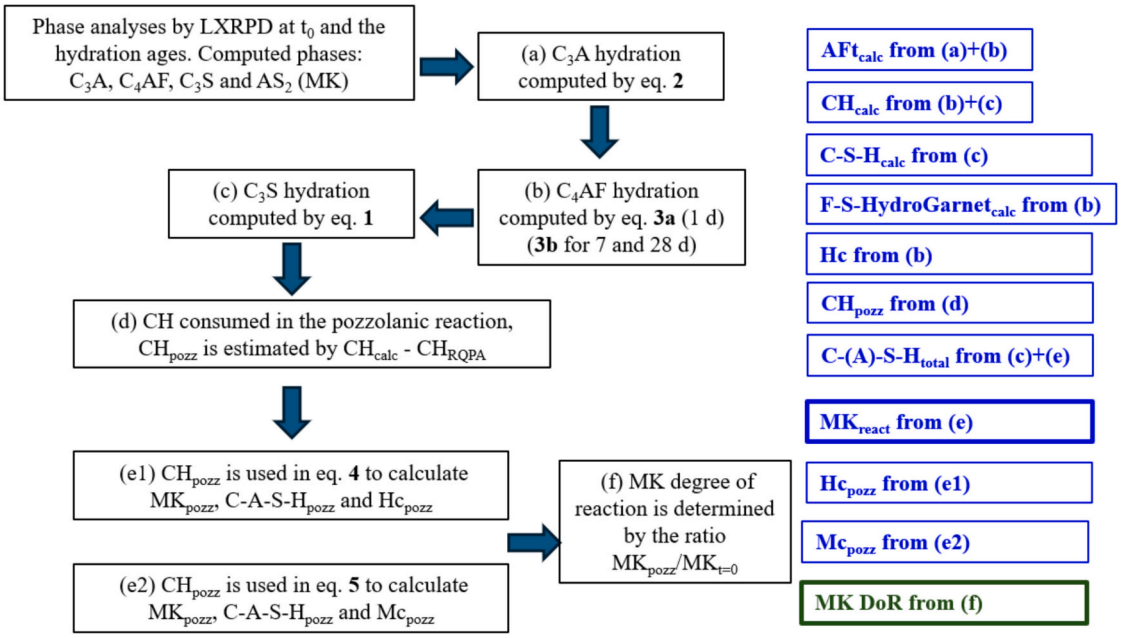

Fig. 7. Flowchart with the steps followed for the mass balance calculations. The stoichiometries of the hydration reactions are given in Table A7.

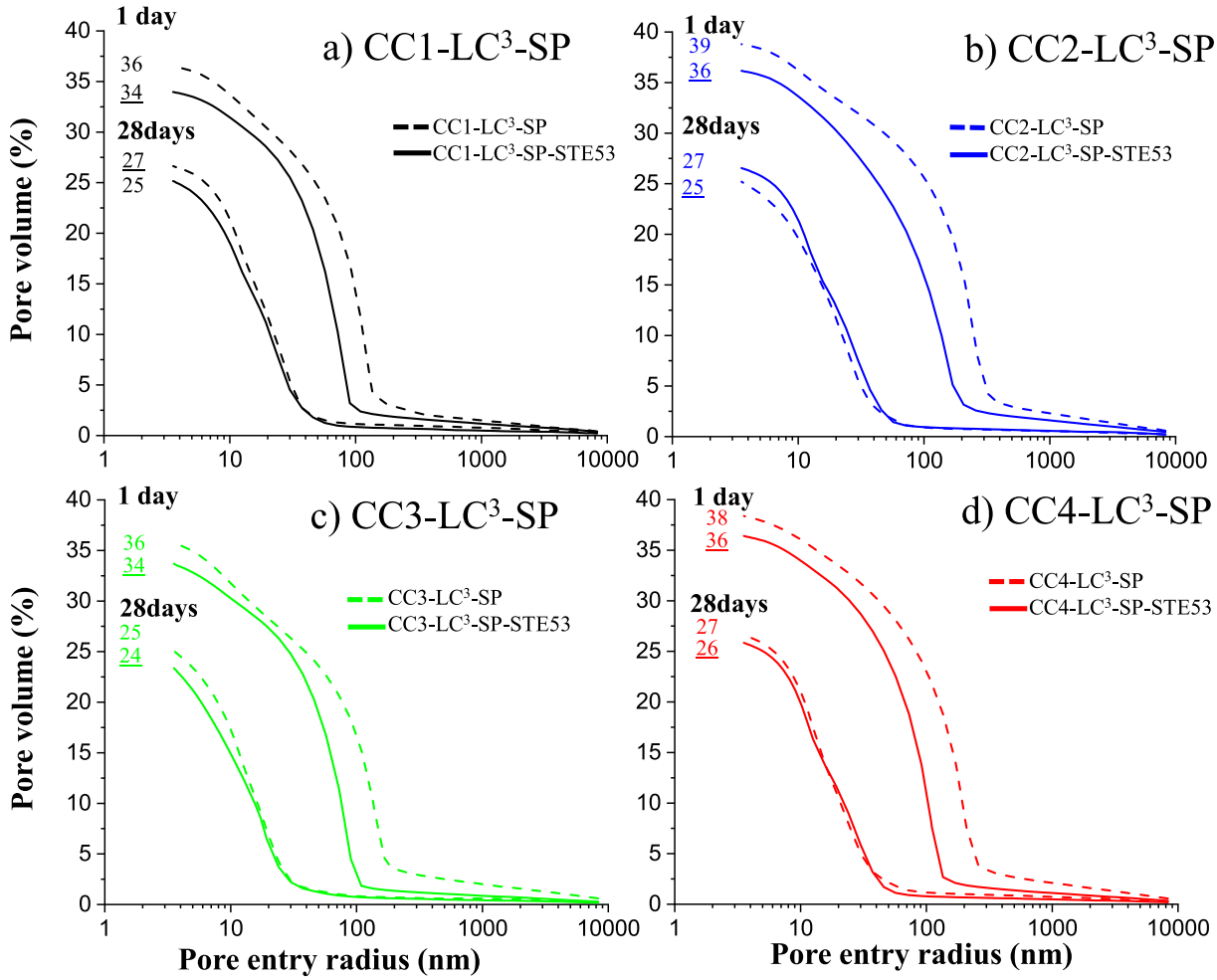

Fig. 8. Cumulative porosity curves for all CCx-LC^3-SP studied pastes at 1 and 28 days of hydration. Unseeded (dashed lines) and seeded with STE53 (continuous lines). Numbers in the inset indicate the total percolated pore volumes (in percentage).

3.5. CC4-LC^3 concrete

The CC4-LC^3 binder was selected for concrete preparation, as detailed in the experimental section, w/b = 0.50. Table 10 provides the SP dosage, initial air content, and slump measurements at different times (t_0, 30, and 60 min) for both unseeded and seeded concretes. It is noted that the slumps of the LC^3-50 concretes did not decrease in the studied time interval. The corresponding values for the concrete fabricated with the same PC are given as references.

Table 10 reports the compressive strengths of the three studied concretes at 1, 7 and 28 days of hydration. As expected, the compressive strength at 1 day of CC4-LC^3-SP concrete, without strength enhancing admixture, was low, i.e. 14 MPa. As expected, the strengths moderately increased with time. Very interestingly and in full agreement with the mortar study, the compressive strength of the same concrete with 2 wt% of STE53 underwent a very notable increase at 1 day, i.e. 19 MPa or 37 % of increase. It is worth noting that this value is just 24 % lower than that of the concrete based on the neat PC 525 but it has a 50 % dilution with a content of 30 wt% of calcined low-grade kaolinitic clay. The compressive strength increase was maintained at 7 and 28 days, although quantitatively lower, see Table 10. This behaviour fully mirrors the trend measured for the corresponding mortar. With these results, the C-S-H seeded LC^3 concrete, based on a calcined low-grade kaolinitic clay, can be classified within C30/37, S4–5 class, which shows medium-strength, good workability and a low CO_2 footprint.

4. Conclusions

This research has aimed to push the limits of LC^3-50 binders by utilising commercially available low-grade kaolinite clays, with contents close to 20 wt%, and C-S-H gel nucleation seeding to produce LC^3 mortars with competitive mechanical properties. The main conclusions are:

1. LC^3-50 mortars prepared with a state-of-the-art superplasticiser did not suffer slump retention within the first 60 min. A correlation

Table 10
Main features of the LC^3-50 ready-mix concrete without and with the strength-enhancing admixture. All studies were carried out at 20 °C.

Concrete	SP (wt%)	Initial air (%)	Slump			Compressive strength (MPa)		
			t_0 (mm)	t_{30} (mm)	t_{60} (mm)	1d	7d	28d
PC-525-SP	0.70	2.1	220	230	220	25.2	38.7	46.0
CC4-LC^3-SP	0.80	2.9	200	210	210	14.0	26.5	33.3
CC4-LC^3-SP-STE53	0.80	2.5	210	220	220	19.2 (+37 %)	31.5 (+19 %)	37.8 (+14 %)

between Fe_2O_3 content in the calcined clay and SP demand to achieve comparable self-flows was observed.
2. Unseeded LC^3-50 mortars (w/b = 0.40), incorporating the clay with the highest Fe_2O_3 and high amorphous content, reached 16 MPa at 1 day (45 % higher than mortars with the other SCMs, ~11 MPa, including the reference clay with twice the metakaolin content).
3. C-S-H gel nucleation seeding enhanced 1-day strengths by 45–110 %, with sustained improvements at 28 days, although quantitatively lower (7–33 %).
4. For LC^3-50 concrete (C30/37, S4–5 type, w/b = 0.50, with CC4), seeding increased 1-day compressive strength by 37 %, reaching 19 MPa at 1 day and 38 MPa at 28 days.
5. The LC^3-50 paste (calorimetry) shows that the STE53 remarkably affect the SCMs with the highest Fe_2O_3 contents, likely due to the alkanolamine content in the admixture. Moreover, quantitative powder diffraction revealed enhanced crystalline C_4AF hydration in seeded systems, and portlandite mass balance calculations suggest 50–60 % metakaolin reaction degree at 28 days.

CRediT authorship contribution statement

Diego Vallina: Formal analysis, Writing – review & editing, Methodology, Investigation. **Isabel Santacruz:** Writing – review & editing, Writing – original draft, Project administration, Validation, Investigation, Supervision, Funding acquisition. **Alejandro Morales-Cantero:** Writing – review & editing, Methodology. **María Dolores Rodríguez-Ruiz:** Methodology, Writing – review & editing, Resources. **Ana Cuesta:** Writing – review & editing. **Angeles G. De la Torre:** Supervision, Funding acquisition, Writing – review & editing. **Alessandro Dalla-Libera:** Investigation, Writing – review & editing. **Pere Borralleras:** Investigation, Writing – review & editing. **Sébastien Dhers:** Writing – review & editing, Investigation. **Peter Schwesig:** Writing – review & editing, Investigation. **Oliver Mazanec:** Writing – review & editing, Investigation, Conceptualization. **Miguel A.G. Aranda:** Writing – original draft, Supervision, Writing – review & editing, Conceptualization.

Declaration of Generative AI and AI-assisted technologies in the writing process

In the preparation of the draft of this work, the authors utilised ChatGPT to improve the readability of the manuscript. After employing this tool, the authors carefully reviewed and edited the content as necessary, assuming full responsibility for the final published version.

Declaration of competing interest

The authors declare the following financial interests/personal relationships which may be considered as potential competing interests:

Isabel Santacruz reports financial support was provided by Spain Ministry of Science and Innovation (co-funded by ERDF).

Master Builders Solutions (MBS) and the research group of University of Malaga had a contractual relationship under the "Low-CO^2 Cement Admixture Activation Study". The employed admixtures (MasterCO2re 3240 and Master X-Seed STE 53) are manufactured and commercialised by MBS. MBS has not set any specific guideline for data analysis and/or reporting. The raw data have been openly shared.

If there are other authors, they declare that they have no known competing financial interests or personal relationships that could have appeared to influence the work reported in this paper.

Acknowledgements

PID2020-114650RB-I00 grant from Ministry of Science and Innovation of Spain, co-funded by ERDF, is gratefully acknowledged. D. Vallina thanks Ministry of Science and Innovation of Spain (PRE2021-099053 doctoral grant). The Escuela de Ingenierías Industriales (Univ. Malaga) is also gratefully recognised, as the mechanical properties were measured there (facility funded by Junta de Andalucía and ERDF (IE19_182 UMA grant)). Funding for open access charge: Univ. Málaga/CBUA.

Appendix A. Annex

Table A1
XRF of all calcined clays (CCx). Reference clays are also shown for the sake of comparison.[#]

	CC_{ref1}	CC_{ref2}	CC1	CC2	CC3	CC4
SiO_2	76.5(3)	81.4(3)	57.7(4)	67.1(4)	61.9(4)	67.2(4)
Al_2O_3	20.5(2)	16.4(2)	30.0(2)	16.4(2)	17.3(2)	16.1(2)
$Fe_2O_3^{(a)}$	0.27(2)	0.21(2)	5.7(2)	7.5(2)	9.8(2)	6.7(2)
CaO	0.10(1)	0.08(1)	1.01(7)	1.45(9)	0.99(7)	1.44(9)
MgO	0.08(2)	0.05(2)	0.8(1)	1.1(1)	2.6(2)	2.0(2)
SO_3	–	–	1.11(6)	0.31(2)	0.06(1)	0.06(1)
Na_2O	–	–	0.60(7)	0.31(4)	0.14(2)	0.09(2)
K_2O	1.4(1)	1.3(1)	3.0(1)	3.4(2)	4.0(2)	3.9(2)
TiO_2	0.17(1)	0.16(1)	1.16(1)	0.78(1)	1.12(1)	0.73(1)
P_2O_5	–	–	0.17(1)	0.16(1)	0.04(1)	0.06(1)
MnO	–	–	–	0.19(1)	0.04(1)	0.05(1)
Others	–	0.01	0.56	0.45	0.46	0.44
Al_2O_3/ SiO_2	0.27	0.20	0.52	0.24	0.28	0.24
LOI*	0.95	0.29	1.16	0.83	1.58	1.22

[#] Values in parentheses are the associated errors. [(a)]Total Fe expressed as Fe_2O_3 weight percent.
* LOI: Loss on Ignition. Dried (105 °C for 2 h) and heated (950 °C for 2 h).

Table A2
RQPA (MoKα$_1$) of calcined clays including the ACn, in weight percentage, including reference. Crystal structure codes of MgO and Maghemite are included.[#]

wt%	CC_{ref1}	CC_{ref2}	CC1	CC2	CC3	CC4
Kaolinite	–	–	0.8(3)	–	–	–
Muscovite	1.7(2)	3.1(2)	23.7(7)	15.3(4)	21.0(5)	17.6(4)
Fe_2O_3	0.1(1)	–	2.1(3)	4.8(1)	3.0(2)	0.7(1)
Illite	–	–	–	–	–	–
Quartz	50.5(1)	52.0(1)	7.5(3)	35.3(2)	27.2(3)	36.7(2)
Pyrophyllite	–	–	17.9(4)	–	–	–
Rutile	–	–	–	0.1(1)	–	–
Dolomite	–	–	–	–	–	–
Microcline	5.8(2)	3.1(3)	–	–	–	–
Anatase	0.1(1)	–	–	–	–	–
MgO*	–	–	–	–	1.0(1)	–
Maghemite*	–	–	–	0.4(1)	–	–
ACn	**42**	**42**	**48**	**44**	**48**	**45**

[#] Values in parentheses are the associated errors.
[*] Crystal structure code (AMCSD): MgO: 0018011, Maghemite: 0020518.

Table A3
Full phase assemblage of CC1-LC^3-SP pastes (1, 7 and 28 days) without and with STE53.[#]

Phases	t_0	CC1 LC^3-SP			CC1-LC^3-SP-STE53		
		1d	7d	28d	1d	7d	28d
C_3S	20.2(1)	5.3(3)	1.0(4)	–	4.9(3)	1.0(3)	–
C_2S	4.2(1)	3.8(3)	3.6(2)	2.6(2)	4.2	3.8(2)	2.1(3)
C_4AF	3.8(1)	0.6(1)	0.4(2)	–	0.3(1)	–	–
C_3A	1.6(1)	0.4(1)	–	–	0.2(1)	–	–
CsH_2	2.4(1)	–	–	–	–	–	–
$CsH_{0.5}$	1.3(1)	–	–	–	–	–	–
Minors	0.7	–	–	–	–	–	–
Cc	12.7(1)	13.2(2)	11.5(2)	11.3(2)	11.5(2)	11.2(2)	10.2(2)
Qz	1.7(3)	1.3(1)	1.3(1)	1.4(2)	1.3(1)	1.3(1)	1.3(1)
Silicates + side phases	6.3	5.5	5.9	5.5	4.9	5.3	5.6
CH	–	2.3(1)	3.9(1)	3.6(2)	3.3(2)	3.7(2)	3.4(2)
AFt	–	1.2(1)	2.4(1)	1.5(1)	1.8(1)	2.0(2)	1.2(2)
Hc	–	–	0.1(1)	0.2(1)	–	–	0.4(1)
Mc	–	–	0.2(1)	0.5(1)	–	0.3(1)	0.8(1)
ACn_T	45.2	66.4	69.7	73.4	67.7	71.2	74.9

[#] Values in parentheses are the associated errors.

Table A4
Full phase assemblage of CC2-LC^3-SP pastes (1, 7 and 28 days) without and with STE53.[#]

Phases	t_0	CC2-LC^3-SP			CC2-LC^3-SP-STE53		
		1d	7d	28d	1d	7d	28d
C_3S	20.2(1)	7.2(3)	0.6(2)	–	5.8(2)	0.9(1)	–
C_2S	4.2(1)	3.3(2)	3.9(3)	3.7(3)	4.0(2)	4.1(3)	2.8(2)
C_4AF	3.8(1)	0.7(1)	0.4(1)	–	0.4(1)	0.4(1)	–
C_3A	1.6(1)	0.3(1)	–	–	0.5(1)	–	–
CsH_2	2.4(1)	–	–	–	–	–	–
$CsH_{0.5}$	1.3(1)	–	–	–	–	–	–
Minors	0.7	–	–	–	–	–	–
Cc	12.7(1)	12.7(1)	11.1(1)	10.7(2)	10.3(1)	10.9(2)	10.4(2)
Qz	7.6(2)	6.5(1)	6.1(1)	6.8(1)	6.1(1)	6.9(1)	7.2(1)
Silicates + side phases	4.2	4.2	3.2	4.1	3.7	3.1	4.6
CH	–	2.4(1)	3.7(1)	3.9(1)	2.8(1)	3.9(1)	3.5(1)
AFt	–	1.0(1)	1.5(1)	1.7(1)	1.0(1)	2.0(1)	1.7(1)
Hc	–	–	0.1(1)	0.1(1)	–	0.1(1)	0.6(1)
Mc	–	–	0.1(1)	0.6(1)	–	0.1(1)	0.6(1)
ACn_T	41.4	61.7	69.4	68.4	65.3	67.6	68.6

[#] Values in parentheses are the associated errors.

Table A5
Full phase assemblage of CC3-LC^3-SP pastes (1, 7 and 28 days) without and with STE53.[#]

Phases	t_0	CC3-LC^3-SP			CC3-LC^3-SP-STE53		
		1d	7d	28d	1d	7d	28d
C_3S	20.2(1)	5.9(3)	0.7(1)	–	5.6(3)	0.8(1)	–
C_2S	4.2(1)	4.1(2)	4.0(2)	3.2(3)	4.2(2)	4.4(2)	2.7(2)
C_4AF	3.8(1)	0.8(1)	0.3(1)	–	0.3(1)	0.1(1)	–
C_3A	1.6(1)	0.2(1)	–	–	–	–	–
CsH_2	2.4(1)	–	–	–	–	–	–
$CsH_{0.5}$	1.3(1)	–	–	–	–	–	–
Minors	0.7	–	–	–	–	–	–
Cc	12.7(1)	12.6(1)	11.2(2)	11.4(2)	11.6(2)	10.3(2)	10.6(2)
Qz	5.8(3)	4.8(1)	4.7(1)	4.2(1)	4.9(1)	4.8(1)	5.1(2)
Silicates + side phases	5.3	6.1	5.4	5.6	4.6	4.9	5.5
CH	–	2.1(1)	3.0(1)	3.4(1)	2.8(1)	3.2(1)	3.0(1)
AFt	–	1.1(1)	1.8(1)	1.8(1)	1.7(1)	1.5(1)	1.6(1)
Hc	–	–	0.1(1)	0.3(1)	–	0.4(1)	0.6(1)
Mc	–	–	0.2(1)	0.6(1)	–	0.3(1)	0.5(1)
ACn_T	42.1	62.4	68.6	69.3	64.3	69.2	70.5

[#] Values in parentheses are the associated errors.

Table A6
Full phase assemblage of CC4- LC^3-SP pastes (1, 7 and 28 days) without and with STE53.[#]

Phases	t_0	CC4-LC^3-SP			CC4-LC^3-SP-STE53		
		1d	7d	28d	1d	7d	28d
C_3S	20.2(1)	5.8(3)	0.6(1)	–	5.5(3)	0.9(1)	–
C_2S	4.2(1)	4.2(3)	4.2(3)	3.4(3)	4.3(3)	3.9(3)	2.6(3)
C_4AF	3.8(1)	0.6(1)	0.4(1)	–	0.5(1)	0.1(1)	–
C_3A	1.6(1)	0.5(1)	–	–	0.3(1)	–	–
CsH_2	2.4(1)	–	–	–	–	–	–
$CsH_{0.5}$	1.3(1)	–	–	–	–	–	–
Minors	0.7	–	–	–	–	–	–
Cc	12.7(1)	11.9(2)	12.0(2)	11.1(2)	12.8(1)	10.4(2)	10.0(2)
Qz	7.9(2)	6.2(1)	6.6(1)	7.0(1)	6.6(1)	6.8(1)	7.3(1)
Silicates + side phases	3.8	4.5	4.3	4.6	4.7	3.7	4.5
CH	–	2.9(1)	3.9(1)	3.6(1)	2.8(1)	3.4(1)	3.6(1)
AFt	–	1.0(1)	2.0(1)	1.8(1)	1.6(1)	2.0(1)	1.3(1)
Hc	–	–	0.2(1)	0.3(1)	–	0.4(1)	0.4(1)
Mc	–	–	0.1(1)	0.6(1)	–	0.3(1)	0.7(1)
ACn_T	41.4	62.5	65.6	67.6	60.9	68.1	69.4

[#] Values in parentheses are the associated errors.

Table A7
Chemical reactions employed for the mass balance calculations.

Reactions	Eq.
$Ca_3SiO_5 + 5.2\ H_2O \rightarrow 1.2\ Ca(OH)_2 + (CaO)_{1.8}SiO_2(H_2O)_{4.0}$	(1)
$Ca_3Al_2O_6 + 3CaSO_4{\cdot}2H_2O + 26\ H_2O \rightarrow Ca_6Al_2(SO_4)_3(OH)_{12}{\cdot}26H_2O$	(2)
$Ca_4Al_2Fe_2O_{10} + 0.84\ Ca_3SiO_5 + 3CaSO_4{\cdot}2H_2O + 30.84\ H_2O \rightarrow Ca_3Fe_2(SiO_4)_{0.84}(OH)_{8.64} + Ca_6Al_2(SO_4)_3(OH)_{12}{\cdot}26H_2O + 0.52\ Ca(OH)_2$	(3a)
$Ca_4Al_2Fe_2O_{10} + 0.84\ Ca_3SiO_5 + 0.5\ CaCO_3 + 16.34\ H_2O \rightarrow Ca_3Fe_2(SiO_4)_{0.84}(OH)_{8.64} + Ca_4Al_2(OH)_{13}(CO_3)_{0.5}(H_2O)_{5.5} + 0.02\ Ca(OH)_2$	(3b)
$Al_2Si_2O_7 + 5.8\ Ca(OH)_2 + 0.4\ CaCO_3 + 11.8\ H_2O \rightarrow 2\ Ca_{1.5}Al_{0.2}SiO_{3.8}(H_2O)_{4.0} + 0.8\ Ca_4Al_2(OH)_{13}(CO_3)_{0.5}(H_2O)_{5.5}$	(4)
$Al_2Si_2O_7 + 5.4\ Ca(OH)_2 + 0.8\ CaCO_3 + 11.4\ H_2O \rightarrow 2\ Ca_{1.5}Al_{0.2}SiO_{3.8}(H_2O)_{4.0} + 0.8\ Ca_4Al_2(OH)_{12}(CO_3)(H_2O)_5$	(5)

Appendix B. Supplementary data

Supplementary data to this article can be found online at https://doi.org/10.1016/j.cemconres.2025.108036.

Data availability

All raw data are available in Zenodo, doi:https://doi.org/10.5281/zenodo.15398054, which can be used under the Creative Commons Attribution license.

Laboratory X-ray powder diffraction (raw and calcined clays, and LC^3 pastes at 1, 7 and 28 days), **thermal analysis** (raw clays, and LC^3 pastes at 1, 7 and 28 days), **particle size distribution by laser diffraction** (calcined clays), **isothermal calorimetry** (R^3 calcined clays, LC^3 pastes), and **mercury intrusion porosimetry** (LC^3 pastes at 1

and 28 days).

References

[1] R. Snellings, P. Suraneni, J. Skibsted, Future and emerging supplementary cementitious materials, Cem. Concr. Res. 171 (2023) 107199, https://doi.org/10.1016/J.CEMCONRES.2023.107199.

[2] M. Sharma, S. Bishnoi, F. Martirena, K. Scrivener, Limestone calcined clay cement and concrete: a state-of-the-art review, Cem. Concr. Res. 149 (2021) 106564, https://doi.org/10.1016/j.cemconres.2021.106564.

[3] UNE-EN 197-5, Parte 5: Cemento Portland compuesto CEM II/C-M y cemento compuesto CEM VI, 2021.

[4] M. Maier, N. Beuntner, K.C. Thienel, Mineralogical characterization and reactivity test of common clays suitable as supplementary cementitious material, Appl. Clay Sci. 202 (2021) 105990, https://doi.org/10.1016/j.clay.2021.105990.

[5] D. Vallina, M.D. Rodríguez-Ruiz, I. Santacruz, A. Cuesta, M.A.G. Aranda, A.G. De la Torre, Supplementary cementitious material based on calcined montmorillonite standards, Construct. Build Mater. 426 (2024) 136193, https://doi.org/10.1016/J.CONBUILDMAT.2024.136193.

[6] S.E. Schulze, J. Rickert, Suitability of natural calcined clays as supplementary cementitious material, Cem. Concr. Compos. 95 (2019) 92–97, https://doi.org/10.1016/j.cemconcomp.2018.07.006.

[7] A. Alujas, R. Fernández, R. Quintana, K.L. Scrivener, F. Martirena, Pozzolanic reactivity of low grade kaolinitic clays: influence of calcination temperature and impact of calcination products on OPC hydration, Appl. Clay Sci. 108 (2015) 94–101, https://doi.org/10.1016/j.clay.2015.01.028.

[8] A. Morales-Cantero, A.G. De la Torre, A. Cuesta, I. Santacruz, O. Mazanec, A. Dalla-Libera, P. Borralleras, M.A.G. Aranda, In situ synchrotron powder diffraction study of LC3 cement activation at very early ages by C-S-H nucleation seeding, Cem. Concr. Res. 178 (2024) 107463, https://doi.org/10.1016/j.cemconres.2024.107463.

[9] K. Weise, N. Ukrainczyk, E. Koenders, Pozzolanic metakaolin reactions: stoichiometric and kinetic modeling, Mater. Des. 239 (2024) 112747, https://doi.org/10.1016/j.matdes.2024.112747.

[10] F. Zunino, Y. Dhandapani, M. Ben Haha, J. Skibsted, S. Joseph, S. Krishnan, A. Parashar, M.C.G. Juenger, T. Hanein, S.A. Bernal, K.L. Scrivener, F. Avet, Hydration and mixture design of calcined clay blended cements: review by the RILEM TC 282-CCL, Mater. Struct. Constr. 55 (2022) 234, https://doi.org/10.1617/s11527-022-02060-1.

[11] M. Antoni, J. Rossen, F. Martirena, K.L. Scrivener, Cement substitution by a combination of metakaolin and limestone, Cem. Concr. Res. 42 (2012) 1579–1589, https://doi.org/10.1016/j.cemconres.2012.09.006.

[12] K. Scrivener, F. Martirena, S. Bishnoi, S. Maity, Calcined clay limestone cements (LC3), Cem. Concr. Res. 114 (2018) 49–56, https://doi.org/10.1016/j.cemconres.2017.08.017.

[13] A. Alujas Diaz, R.S. Almenares Reyes, T. Hanein, E.F. Irassar, M. Juenger, F. Kanavaris, M. Maier, A.T. Marsh, T. Sui, K.C. Thienel, L. Valentini, B. Wang, F. Zunino, R. Snellings, Properties and occurrence of clay resources for use as supplementary cementitious materials: a paper of RILEM TC 282-CCL, Mater. Struct. Constr. 55 (2022), https://doi.org/10.1617/s11527-022-01972-2.

[14] A. Alujas Díaz, R.S. Almenares-Reyes, F.A. Carratalá, J.F. Martirena Hernández, Proposal of a methodology for the preliminary assessment of kaolinitic clay deposits as a source of SCMsTitle, in: F. Martirena, A. Favier, K. Scrivener (Eds.), Calcined Clays Sustain. Concr. Proc. 2nd Int. Conf. Calcined Clays Sustain, Concr., Springer, 2018, pp. 29–34, https://doi.org/10.1007/978-94-024-1207-9_5.

[15] H. Ghorbel, B. Samet, Effect of iron on pozzolanic activity of kaolin, Construct. Build Mater. 44 (2013) 185–191, https://doi.org/10.1016/J.CONBUILDMAT.2013.02.068.

[16] M.U. Rehman, M. Ahmad, K. Rashid, Influence of fluxing oxides from waste on the production and physico-mechanical properties of fired clay brick: a review, J. Build. Eng. 27 (2020) 100965, https://doi.org/10.1016/J.JOBE.2019.100965.

[17] R. Snellings, R. Almenares Reyes, T. Hanein, E.F. Irassar, F. Kanavaris, M. Maier, A. T. Marsh, L. Valentini, F. Zunino, A. Alujas Diaz, Paper of RILEM TC 282-CCL: mineralogical characterization methods for clay resources intended for use as supplementary cementitious material, Mater. Struct. Constr. 55 (2022) 1–32, https://doi.org/10.1617/s11527-022-01973-1.

[18] I.M.R. Bernal, M.A.G. Aranda, I. Santacruz, A.G. De la Torre, A. Cuesta, Early-age reactivity of calcined kaolinitic clays in LC3 cements: a multi technique study including pair distribution function analysis, J. Sustain. Cem. Mater. 12 (2023) 721–735, https://doi.org/10.1080/21650373.2022.2117248.

[19] F. Avet, K.L. Scrivener, Investigation of the calcined kaolinite content on the hydration of Limestone Calcined Clay Cement (LC3), Cem. Concr. Res. 107 (2018) 124–135, https://doi.org/10.1016/j.cemconres.2018.02.016.

[20] S. Dhers, A. Müller, R. Guggenberger, D. Freimut, K. Weldert, B. Sachsenhauser, V. Yermakou, N. Mikanovic, P. Schwesig, On the relationship between superplasticizer demand and specific surface area of calcined clays in LC3 systems, Construct. Build Mater. 411 (2024) 134467, https://doi.org/10.1016/J.CONBUILDMAT.2023.134467.

[21] J. Mañosa, S. Huete-Hernández, A. Alvarez-Coscojuela, A. Maldonado-Alameda, J. M. Chimenos, Comparative study of limestone calcined clay cement produced with mechanically activated kaolin and calcined kaolin, J. Build. Eng. 97 (2024) 110748, https://doi.org/10.1016/j.jobe.2024.110748.

[22] K.L. Scrivener, F. Avet, H. Maraghechi, F. Zunino, J. Ston, W. Hanpongpun, A. Favier, Impacting factors and properties of limestone calcined clay cements (LC3), Green Mater. 7 (2019) 3–14, https://doi.org/10.1680/jgrma.18.00029.

[23] K. Ram, M. Flegar, M. Serdar, K. Scrivener, Influence of low- to medium-kaolinite clay on the durability of limestone calcined clay cement (LC3) concrete, Mater. 2023 16 (2022) 374, https://doi.org/10.3390/MA16010374.

[24] B. Ayati, D. Newport, H. Wong, C. Cheeseman, Low-carbon cements: potential for low-grade calcined clays to form supplementary cementitious materials, Clean. Mater. 5 (2022) 100099, https://doi.org/10.1016/j.clema.2022.100099.

[25] N. Blouch, K. Rashid, I. Zafar, M. Ltifi, M. Ju, Prioritization of low-grade kaolinite and mixed clays for performance evaluation of Limestone Calcined Clay Cement (LC3): multi-criteria assessment, Appl. Clay Sci. 243 (2023) 107080, https://doi.org/10.1016/J.CLAY.2023.107080.

[26] N. Blouch, K. Rashid, M. Ju, Exploring low-grade clay minerals diving into limestone calcined clay cement (LC3): characterization – hydration – performance, J. Clean. Prod. 426 (2023) 139065, https://doi.org/10.1016/j.jclepro.2023.139065.

[27] A. Zolfagharnasab, A.A. Ramezanianpour, F. Bahman-Zadeh, Investigating the potential of low-grade calcined clays to produce durable LC3 binders against chloride ions attack, Construct. Build Mater. 303 (2021) 124541, https://doi.org/10.1016/j.conbuildmat.2021.124541.

[28] H. Maraghechi, F. Avet, H. Wong, H. Kamyab, K.L. Scrivener, Performance of Limestone Calcined Clay Cement (LC3) with various kaolinite contents with respect to chloride transport, Mater. Struct. 51 (2018) 125, https://doi.org/10.1617/s11527-018-1255-3.

[29] A. Dixit, H. Du, S.D. Pang, Performance of mortar incorporating calcined marine clays with varying kaolinite content, J. Clean. Prod. 282 (2021) 124513, https://doi.org/10.1016/j.jclepro.2020.124513.

[30] G. Cardinaud, E. Rozière, O. Martinage, A. Loukili, L. Barnes-Davin, M. Paris, D. Deneele, Calcined clay – limestone cements: hydration processes with high and low-grade kaolinite clays, Construct. Build Mater. 277 (2021) 122271, https://doi.org/10.1016/j.conbuildmat.2021.122271.

[31] A.H. Ahmed, S. Nune, M. Liebscher, T. Köberle, A. Willomitzer, I. Noack, M. Butler, V. Mechtcherine, Exploring the role of dilutive effects on microstructural development and hydration kinetics of limestone calcined clay cement (LC3) made of low-grade raw materials, J. Clean. Prod. 428 (2023) 139438, https://doi.org/10.1016/j.jclepro.2023.139438.

[32] R. Hay, K. Celik, Performance enhancement and characterization of limestone calcined clay cement (LC3) produced with low-reactivity kaolinitic clay, Constr. Build. Mater. 392 (2023) 131831, https://doi.org/10.1016/j.conbuildmat.2023.131831.

[33] Y. Dhandapani, A.T.M. Marsh, S. Rahmon, F. Kanavaris, A. Papakosta, S.A. Bernal, Suitability of excavated London clay as a supplementary cementitious material: mineralogy and reactivity, Mater. Struct. Constr. 56 (2023) 174, https://doi.org/10.1617/s11527-023-02260-3.

[34] ASTM, C1897-20 Standard Test Methods for Measuring the Reactivity of Supplementary Cementitious Materials by Isothermal Calorimetry and Bound Water Measurements, 2020, https://doi.org/10.1520/C1897-20.

[35] Y. Dhandapani, T. Sakthivel, M. Santhanam, R. Gettu, R.G. Pillai, Mechanical properties and durability performance of concretes with limestone calcined clay cement (LC3), Cem. Concr. Res. 107 (2018) 136–151, https://doi.org/10.1016/J.CEMCONRES.2018.02.005.

[36] S. Al-Shmaisani, R.D. Kalina, R.D. Ferron, M.C.G. Juenger, Critical assessment of rapid methods to qualify supplementary cementitious materials for use in concrete, Cem. Concr. Res. 153 (2022) 106709, https://doi.org/10.1016/J.CEMCONRES.2021.106709.

[37] E. John, T. Matschei, D. Stephan, Nucleation seeding with calcium silicate hydrate – a review, Cem. Concr. Res. 113 (2018) 74–85, https://doi.org/10.1016/j.cemconres.2018.07.003.

[38] G. Artioli, G. Ferrari, M.C. Dalconi, L. Valentini, Nanoseeds as modifiers of the cement hydration kinetics, in: M. Shahir Liew, P. Nguyen-Tri, T.A. Nguyen, S. Kakooei (Eds.), Smart Nanoconcretes Cem. Mater. Prop. Model. Appl., Elsevier, 2020, pp. 257–269, https://doi.org/10.1016/B978-0-12-817854-6.00010-6.

[39] A. Cuesta, A. Morales-Cantero, A.G. De la Torre, M.A.G. Aranda, Recent advances in C-S-H nucleation seeding for improving cement performances, Materials (Basel). 16 (2023) 1462, https://doi.org/10.3390/ma16041462.

[40] L. Nicoleau, E. Schreiner, A. Nonat, Ion-specific effects influencing the dissolution of tricalcium silicate, Cem. Concr. Res. 59 (2014) 118–138, https://doi.org/10.1016/j.cemconres.2014.02.006.

[41] E. Pustovgar, R.K. Mishra, M. Palacios, J.-B. d'Espinose de Lacaillerie, T. Matschei, A.S. Andreev, H. Heinz, R. Verel, R.J. Flatt, Influence of aluminates on the hydration kinetics of tricalcium silicate, Cem. Concr. Res. 100 (2017) 245–262, https://doi.org/10.1016/j.cemconres.2017.06.006.

[42] D. Wagner, F. Bellmann, J. Neubauer, Influence of aluminium on the hydration of triclinic C3S with addition of KOH solution, Cem. Concr. Res. 137 (2020) 106198, https://doi.org/10.1016/j.cemconres.2020.106198.

[43] T. Hirsch, Z. Lu, D. Stephan, Effect of different sulphate carriers on Portland cement hydration in the presence of triethanolamine, Constr. Build. Mater. 294 (2021) 123528, https://doi.org/10.1016/j.conbuildmat.2021.123528.

[44] C. Redondo-Soto, D. Gastaldi, S. Irico, F. Canonico, M.A.G. Aranda, Belite clinkers with increasing aluminium content: effect of calcium aluminates on calcium silicate hydration, Cem. Concr. Res. 162 (2022) 107015, https://doi.org/10.1016/j.cemconres.2022.107015.

[45] E.M.J. Bérodier, A.C.A. Muller, K.L. Scrivener, Effect of sulfate on C-S-H at early age, Cem. Concr. Res. 138 (2020) 106248, https://doi.org/10.1016/j.cemconres.2020.106248.

[46] W. Li, M. Fall, Sulphate effect on the early age strength and self-desiccation of cemented paste backfill, Construct. Build Mater. 106 (2016) 296–304, https://doi.org/10.1016/J.CONBUILDMAT.2015.12.124.

[47] A. Morales-Cantero, A.G. De la Torre, A. Cuesta, I. Santacruz, O. Mazanec, A. Dalla-Libera, S. Dhers, P. Borralleras, M.A.G. Aranda, Activation of LC3 low-carbon cements by C-S-H seeding, in: Proc. 16th Int. Congr. Chem. Cem vol I, 2023, pp. 247–250, https://doi.org/10.13140/RG.2.2.26594.09920. Bangkok.

[48] A. Morales-Cantero, A. Cuesta, A.G. De la Torre, I. Santacruz, O. Mazanec, P. Borralleras, K.S. Weldert, D. Gastaldi, F. Canonico, M.A.G. Aranda, C-S-H seeding activation of portland and belite cements: an enlightening in situ synchrotron powder diffraction study, Cem. Concr. Res. 161 (2022) 106946, https://doi.org/10.1016/j.cemconres.2022.106946.

[49] A. Cuesta, A. Morales-Cantero, A.G. De la Torre, I. Santacruz, O. Mazanec, A. Dalla-Libera, S. Dhers, P. Schwesig, P. Borralleras, M.A.G. Aranda, Activation of LC3 binders by C-S-H nucleation seeding with a new tailored admixture for low-carbon cements, Ce/Papers - Proc. Civ. Eng. 6 (2023) 446–453, https://doi.org/10.1002/cepa.2786.

[50] S. Shirani, A. Cuesta, A. Morales-Cantero, I. Santacruz, A. Diaz, P. Trtik, M. Holler, A. Rack, B. Lukic, E. Brun, I.R. Salcedo, M.A.G. Aranda, 4D nanoimaging of early age cement hydration, Nat. Commun. 14 (2023) 2652, https://doi.org/10.1038/s41467-023-38380-1.

[51] A. Kumar, T. Oey, G. Falzone, J. Huang, M. Bauchy, M. Balonis, N. Neithalath, J. Bullard, G. Sant, The filler effect: the influence of filler content and type on the hydration rate of tricalcium silicate, J. Am. Ceram. Soc. 100 (2017) 3316–3328, https://doi.org/10.1111/JACE.14859.

[52] T. Oey, A. Kumar, J.W. Bullard, N. Neithalath, G. Sant, The filler effect: the influence of filler content and surface area on cementitious reaction rates, J. Am. Ceram. Soc. 96 (2013) 1978–1990, https://doi.org/10.1111/jace.12264.

[53] E. Berodier, K.L. Scrivener, Understanding the filler effect on the nucleation and growth of C-S-H, J. Am. Ceram. Soc. 97 (2014) 3764–3773, https://doi.org/10.1111/jace.13177.

[54] G. Artioli, L. Valentini, M.C. Dalconi, M. Parisatto, M. Voltolini, V. Russo, G. Ferrari, Imaging of nano-seeded nucleation in cement pastes by X-ray diffraction tomography, Int. J. Mater. Res. 105 (2014) 628–631, https://doi.org/10.3139/146.111049.

[55] S. Shirani, A. Cuesta, I. Santacruz, A.G. De la Torre, A. Diaz, P. Trtik, M. Holler, M. A.G. Aranda, X-ray near-field ptychographic nanoimaging of cement pastes, Cem. Concr. Res. 185 (2024) 107622, https://doi.org/10.1016/j.cemconres.2024.107622.

[56] D. Zhao, R. Khoshnazar, Hydration and microstructural development of calcined clay cement paste in the presence of calcium-silicate-hydrate (C–S–H) seed, Cem. Concr. Compos. 122 (2021) 104162, https://doi.org/10.1016/j.cemconcomp.2021.104162.

[57] L. Valentini, G. Ferrari, V. Russo, M. Štefančič, V.Z. Serjun, G. Artioli, Use of nanocomposites as permeability reducing admixtures, J. Am. Ceram. Soc. 101 (2018) 4275–4284, https://doi.org/10.1111/JACE.15548.

[58] A. Morales-Cantero, A. Cuesta, A.G. De la Torre, O. Mazanec, P. Borralleras, K. S. Weldert, D. Gastaldi, F. Canonico, M.A.G. Aranda, Portland and belite cement hydration acceleration by C-S-H seeds with variable w/c ratios, Materials (Basel). 15 (2022) 3553, https://doi.org/10.3390/MA15103553.

[59] A. Morales-Cantero, D. Vallina, A.G. De la Torre, A. Cuesta, I. Santacruz, A. Dalla-Libera, P. Borralleras, S. Dhers, P. Schwesig, O. Mazanec, M.A.G. Aranda, Enhancing fluidity and mechanical properties in limestone calcined clay cements with one-third Portland clinker content, J. Build. Eng. 95 (2024) 110334, https://doi.org/10.1016/j.jobe.2024.110334.

[60] D. Vallina, M.D. Rodríguez-Ruiz, A. Morales-Cantero, A. Cuesta, I. Santacruz, A. Dalla-Libera, P. Borralleras, S. Dhers, P. Schwesig, O. Mazanec, M.A.G. Aranda, A.G. De la Torre, Bentonite-based LC3 low carbon cement and activation by C-S-H nucleation seeding, Cem. Concr. Compos. 160 (2025) 106073, https://doi.org/10.1016/J.CEMCONCOMP.2025.106073.

[61] A.G. De la Torre, S. Bruque, M.A.G. Aranda, Rietveld quantitative amorphous content analysis, J. Appl. Cryst. 34 (2001) 196–202, https://doi.org/10.1107/S0021889801002485.

[62] R. Snellings, J. Chwast, Ö. Cizer, N. De Belie, Y. Dhandapani, P. Durdzinski, J. Elsen, J. Haufe, D. Hooton, C. Patapy, M. Santhanam, K. Scrivener, D. Snoeck, L. Steger, S. Tongbo, A. Vollpracht, F. Winnefeld, B. Lothenbach, Report of TC 238-SCM: hydration stoppage methods for phase assemblage studies of blended cements—results of a round robin test, Mater. Struct. Constr. 51 (2018), https://doi.org/10.1617/s11527-018-1237-5.

[63] A.C. Larson, R.B. Von Dreele, General structure analysis system (GSAS), Los Alamos Natl. Lab. Rep. LAUR 748 (2004) 86–748.

[64] B.H. Toby, EXPGUI, a graphical user interface for GSAS, J. Appl. Cryst. 34 (2001) 210–213, https://doi.org/10.1107/S0021889801002242.

[65] D. Londono-Zuluaga, A. Gholizadeh-Vayghan, F. Winnefeld, F. Avet, M. Ben Haha, S.A. Bernal, Ö. Cizer, M. Cyr, S. Dolenec, P. Durdzinski, J. Haufe, D. Hooton, S. Kamali-Bernard, X. Li, A.T.M. Marsh, M. Marroccoli, M. Mrak, Y. Muy, C. Patapy, M. Pedersen, S. Sabio, S. Schulze, R. Snellings, A. Telesca, A. Vollpracht, G. Ye, S. Zhang, K.L. Scrivener, Report of RILEM TC 267-TRM phase 3: validation of the R3 reactivity test across a wide range of materials, Mater. Struct. Constr. 55 (2022) 1–16, https://doi.org/10.1617/s11527-022-01947-3.

[66] J. Sun, F. Zunino, K. Scrivener, Hydration and phase assemblage of limestone calcined clay cements (LC3) with clinker content below 50%, Cem. Concr. Res. 177 (2024) 107417 https://doi.org/10.1016/j.cemconres.2023.107417.

[67] R.G. Pillai, R. Gettu, M. Santhanam, S. Rengaraju, Y. Dhandapani, S. Rathnarajan, A.S. Basavaraj, Service life and life cycle assessment of reinforced concrete systems with limestone calcined clay cement (LC3), Cem. Concr. Res. 118 (2019) 111–119, https://doi.org/10.1016/J.CEMCONRES.2018.11.019.

[68] L.M. Vizcaíno-Andrés, S. Sánchez-Berriel, S. Damas-Carrera, A. Pérez-Hernández, K.L. Scrivener, J.F. Martirena-Hernández, Industrial trial to produce a low clinker, low carbon cement, Mater. Constr. 65 (2015) e045, https://doi.org/10.3989/mc.2015.00614.

[69] EFCA, European Federation of Concrete Admixtures Associations. https://www.efca.info/efca-publications/environmental/, 2023.

[70] MasterCO2re 3240. https://assets.ctfassets.net/ctspkgm1yw3s/3X1W84AEOGKtMyzHFEHh7J/73fbee217e51b59040fd791defd35c63/MasterCO2re_3240_EFCA-mEPD_Group_B.pdf, 2024.

[71] Master X-Seed STE 54. https://assets.ctfassets.net/ctspkgm1yw3s/2fNa9BdTRv4wzpLBoKXOUd/3bf8c957c5441f5362e5b79e98e6cdc5/Master_X-Seed_STE_54_EPD_2027-07-21.pdf, 2024.

[72] I. Wadsö, Isothermal microcalorimetry near ambient temperature: an overview and discussion, Thermochim. Acta 294 (1997) 1–11, https://doi.org/10.1016/S0040-6031(96)03136-X.

[73] A. Mezhov, D. Kulisch, A. Goncharov, S. Zhutovsky, A comparative study of factors influencing hydration stoppage of hardened cement paste, Sustain 15 (2023) 1080, https://doi.org/10.3390/su15021080.

[74] K. Thienel, S. Scherb, N. Beuntner, M. Maier, R. Sposito, 1:1 or 2:1 - Does it matter for calcined clay as supplementary cementitious material? Ce/Papers - Proc. Civ. Eng. (2023) 363–372, https://doi.org/10.1002/cepa.2775.

[75] T. Hanein, K.-C. Thienel, F. Zunino, A.T.M. Marsh, M. Maier, B. Wang, M. Canut, M.C.G. Juenger, M. Ben Haha, F. Avet, A. Parashar, L.A. Al-Jaberi, R.S. Almenares-Reyes, A. Alujas-Diaz, K.L. Scrivener, S.A. Bernal, J.L. Provis, T. Sui, S. Bishnoi, F. Martirena-Hernández, Clay calcination technology: state-of-the-art review by the RILEM TC 282-CCL, Mater. Struct. 55 (2021) 1–29, https://doi.org/10.1617/S11527-021-01807-6.

[76] L.N. Warr, IMA–CNMNC approved mineral symbols, Mineral. Mag. 85 (2021) 291–320, https://doi.org/10.1180/MGM.2021.43.

[77] M. Földvári, Handbook of Thermogravimetric System of Minerals and Its Use in Geological Practice: Occasional Papers of the Geological Institute of Hungary 213, 2011, p. 180.

[78] L. Wang, M. Zhang, S.A.T. Redfern, Z. Zhang, Dehydroxylation and transformations of the 2:1 phyllosilicate pyrophyllite at elevated temperatures: an infrared spectroscopic study, Clays Clay Miner. 50 (2002) 272–283, https://doi.org/10.1346/000986002760832874.

[79] I. Koufany, I. Santacruz, M.-D. Rodriguez-Ruiz, E. Bescher, M.A.G. Aranda, A.G. De la Torre, Effect of alkanolamines in kaolinitic calcined clays pozzolanic reactivity, Proc. 16th Int. Congr. Chem. Cem. (2023), https://doi.org/10.13140/RG.2.2.35533.20960.

[80] F. Avet, R. Snellings, A. Alujas Diaz, M. Ben Haha, K.L. Scrivener, Development of a new rapid, relevant and reliable (R3) test method to evaluate the pozzolanic reactivity of calcined kaolinitic clays, Cem. Concr. Res. 85 (2016) 1–11, https://doi.org/10.1016/j.cemconres.2016.02.015.

[81] F. Avet, X. Li, M. Ben Haha, S.A. Bernal, S. Bishnoi, Ö. Cizer, M. Cyr, S. Dolenec, P. Durdzinski, J. Haufe, D. Hooton, M.C.G. Juenger, S. Kamali-Bernard, D. Londono-Zuluaga, A.T.M. Marsh, M. Marroccoli, M. Mrak, A. Parashar, C. Patapy, M. Pedersen, J.L. Provis, S. Sabio, S. Schulze, R. Snellings, A. Telesca, M. Thomas, F. Vargas, A. Vollpracht, B. Walkley, F. Winnefeld, G. Ye, S. Zhang, K. Scrivener, Report of RILEM TC 267-TRM phase 2: optimization and testing of the robustness of the R3 reactivity tests for supplementary cementitious materials, Mater. Struct. Constr. 55 (2022) 1–14, https://doi.org/10.1617/s11527-022-01928-6.

[82] Intelligent Cluster System. https://info.master-builders-solutions.com/en/masterco2re, 2024.

[83] S.M. Mansour, Behavior of self- compacting concrete incorporating calcined pyrophyllite as supplementary cementitious material, J. Build. Mater. Struct. 7 (2020) 119–129, https://doi.org/10.34118/jbms.v7i1.744.

[84] F. Zunino, K.L. Scrivener, The influence of the filler effect on the sulfate requirement of blended cements, Cem. Concr. Res. 126 (2019) 105918, https://doi.org/10.1016/j.cemconres.2019.105918.

[85] V. Shah, A. Parashar, G. Mishra, S. Medepalli, S. Krishnan, S. Bishnoi, Influence of cement replacement by limestone calcined clay pozzolan on the engineering properties of mortar and concrete, Adv. Cem. Res. 32 (2020) 101–111, https://doi.org/10.1680/JADCR.18.00073.

[86] M. Panzer, S. Scherb, N. Beuntner, K.C. Thienel, Effect of sulfate carrier addition on the strength of calcined clay blended cements, Constr. Build. Mater. 477 (2025) 140915, https://doi.org/10.1016/j.conbuildmat.2025.140915.

[87] K.L. Scrivener, R. Snellings, B. Lothenbach, A Practical Guide to Microstructural Analysis of Cementitious Materials, CRC Press, Boca Raton, FL, 2017, https://doi.org/10.1201/b19074.

[88] P. Hemstad, B. Lothenbach, K. De Weerdt, Cement and concrete research distribution of sulphate and aluminium in hydrated cement pastes, Cem. Concr. Res. 180 (2024) 107467, https://doi.org/10.1016/j.cemconres.2024.107467.

[89] S. Shirani, A. Cuesta, A.G. De la Torre, I. Santacruz, A. Morales-Cantero, I. Koufany, C. Redondo-Soto, I.R. Salcedo, L. León-Reina, M.A.G. Aranda, Mix and measure - combining in situ X-ray powder diffraction and microtomography for accurate hydrating cement studies, Cem. Concr. Res. 175 (2024) 107370, https://doi.org/10.1016/J.CEMCONRES.2023.107370.

[90] J. Fernandez-Sanchez, A. Cuesta, S. Shirani, C. Redondo-Soto, A.G. De la Torre, I. Santacruz, I.R. Salcedo, L. Leon-Reina, M.A.G. Aranda, Mix and measure II: joint high-energy laboratory powder diffraction and microtomography for cement hydration studies, J. Appl. Cryst. 57 (2024) 1067–1084, https://doi.org/10.1107/s1600576724004527.